

Article

Evaluating the Urban Heat Island Effect in Montreal: Urban Density, Vegetation, Demographic, and Thermal Landscape Analysis

Yassine Hedeya, Abdelatif Merabtine  and Wahid Maref * 

École de Technologie Supérieure (ÉTS), University of Québec, 1100 Rue Notre-Dame Ouest, Montreal, QC H3C 1K3, Canada; yassine.hedeya.1@ens.etsmtl.ca (Y.H.); abdelatif.merabtine@etsmtl.ca (A.M.)

* Correspondence: wahid.maref@etsmtl.ca

Abstract: Montreal experiences a significant urban heat island (UHI) effect, potentially intensified by its dense urban structure, varied vegetation, and demographic distribution, leading to substantial outdoor thermal discomfort, especially during heatwaves. To quantify this, measured thermal landscape data were analyzed over several months in Montreal, including heatwave periods, and outdoor thermal comfort was assessed using the humidex, discomfort index, heat index, and temperature–humidity index. The results indicated notable temperature and humidity variations across the city, with the exceedance of thermal comfort index thresholds being significantly higher during heatwaves (humidex: 10.83%, discomfort index: 53.33%, heat index: 24.77%, temperature–humidity index: 36.67%) compared to normal periods. This study provides a quantitative evaluation of UHI-induced outdoor thermal discomfort in Montreal, emphasizing its severity during heatwaves and analyzing the influence of urban density, vegetation, and anthropogenic emissions, thus offering valuable insights for urban planning strategies to mitigate public health impacts.

Keywords: urban heat island; thermal comfort; heatwave; land surface temperature; urban density; demographics; green spaces



Academic Editors: Tao Luo,
Tingting Hong and Jon Burley

Received: 10 March 2025

Revised: 22 April 2025

Accepted: 26 April 2025

Published: 6 May 2025

Citation: Hedeya, Y.; Merabtine, A.; Maref, W. Evaluating the Urban Heat Island Effect in Montreal: Urban Density, Vegetation, Demographic, and Thermal Landscape Analysis. *Buildings* **2025**, *15*, 1562. <https://doi.org/10.3390/buildings15091562>

Copyright: © 2025 by the authors. Licensee MDPI, Basel, Switzerland. This article is an open access article distributed under the terms and conditions of the Creative Commons Attribution (CC BY) license (<https://creativecommons.org/licenses/by/4.0/>).

1. Introduction

The phenomenon of urbanization profoundly disrupts the natural surface energy balance, leading to a significant increase in both air and surface temperatures within urban environments when compared to their surrounding rural counterparts [1]. This fundamental alteration of the thermal landscape gives rise to the well-documented Urban Heat Island (UHI) effect, a complex meteorological phenomenon with far-reaching consequences for both ecological systems and the immediate outdoor thermal comfort experienced by urban dwellers. Beyond its impact on human comfort, UHI is a significant contributor to the degradation of urban air quality [2], exacerbating the formation of ground-level ozone and increasing the concentration of other harmful pollutants. More critically, UHI directly affects the well-being and health of urban populations, particularly during periods of intense heat, by substantially increasing the risks associated with heatwaves [3,4]. These elevated temperatures can lead to a range of heat-related illnesses, placing a significant strain on public health infrastructure and, in severe cases, contributing to an alarming escalation in mortality rates [5–7].

The relentless pace of global population growth, coupled with the massive and often sprawling development of new urban neighborhoods, has resulted in an alarming and continuous reduction in vital green spaces within and around cities [8,9]. These green

spaces, including parks, forests, and even smaller vegetated areas, play a crucial and multifaceted role in regulating urban temperatures and significantly improving the overall quality of life for city dwellers. Through processes like evapotranspiration and shading, vegetation helps to cool the surrounding environment. The disappearance of these natural cooling mechanisms due to urbanization directly amplifies the effect of UHI, making cities increasingly vulnerable to the adverse impacts of climate change and extreme heat events. This vulnerability underscores the urgent need for a comprehensive understanding of UHI and effective strategies for its mitigation.

To effectively address the multifaceted challenges posed by the UHI effect, it is essential to develop a more nuanced and comprehensive understanding of its underlying mechanisms and the various factors that significantly influence its intensity. This involves a detailed identification of not only the aggravating elements that contribute to UHI, such as high-density urbanization characterized by extensive impervious surfaces and the widespread use of thermally inefficient building and paving materials, but also the exploration and implementation of potential solutions. These solutions may include the strategic integration of green spaces and water bodies within the urban fabric, the adoption of sustainable and heat-reflective urban practices and materials, and innovative urban planning strategies designed to minimize heat retention. Robust research aimed at thoroughly analyzing this complex phenomenon is a critical prerequisite for the development and implementation of more effective and targeted mitigation strategies. A deeper and more nuanced understanding of these intricate thermal dynamics will ultimately promote more thoughtful and sustainable urbanization practices, placing resilience and environmental well-being at the very heart of urban development priorities.

The fundamental definition of the UHI effect as the occurrence of higher surface temperatures in urban environments compared to surrounding rural areas is well-established. However, the precise quantification of its intensity, often represented by the Surface Urban Heat Island Intensity (SUHII) as the temperature difference between urban and rural land surface temperatures (LST urban–LST rural) [10,11], remains a complex and context-dependent endeavor. Despite the considerable body of research already conducted on this critical topic, the comprehensive identification and thorough understanding of the multitude of parameters that interact with and influence UHIs are areas that still require significant development and refinement. Notably, recent studies have begun to highlight the intricate and often synergistic interactions between UHIs and other climate phenomena, such as heatwaves. The study led by Zhao et al. [12] provided compelling evidence of a synergistic interaction between UHIs and heatwaves (HW), suggesting that these two phenomena can amplify each other's negative impacts. This finding was further corroborated by the research of Kim et al. [13], who not only confirmed Zhao et al.'s findings but also sought to delve deeper into the differential effects of various types of heatwaves, specifically distinguishing between arid and humid heatwaves. Their investigation utilized extensive meteorological data spanning the period from 2001 to 2022, along with a range of thermal comfort indices, including humidex, wet-bulb temperature, discomfort index, and Heat index, to comprehensively assess heat stress during these extreme weather events. The results of their study revealed a synergistic interaction between UHIs and arid heatwaves (DHW), while surprisingly indicating a negative interaction between UHIs and humid heatwaves (MHW). Furthermore, the study highlighted the concerning finding that heat stress during nighttime periods associated with DHW can be as severe as, or even more severe than, that experienced during MHW.

To further evaluate this complex interaction between UHI and heatwaves, Shu et al. [14] employed a rigorous methodological procedure that involved a detailed comparison of the urban climate conditions before, during, and after the occurrence of a heatwave.

The determination of the temporal framework for the periods before and after the heatwave followed carefully considered criteria: these periods needed to be sufficiently long (at least two days) to capture baseline conditions but not excessively long (less than two weeks) to avoid the confounding effects of broader seasonal changes. The calculation of the UHI intensity in their study was performed using two distinct methodological approaches: the Rural Ring (RR) method, which involves a direct comparison between urban and surrounding rural environments, and the Urban Increment (UI) method, which compares the existing urban area with a simulation of the same area hypothetically replaced with cropland. Both surface temperature and air temperature data were meticulously taken into account in their analysis. The results of their research demonstrated that the UHI intensity calculated using the UI Method consistently yielded higher values than that obtained through the RR method. Additionally, this study concluded that urban surface coverage has a significant impact not only on the climate within the city itself but also on the climatic conditions of its immediate surroundings. Interestingly, their findings also indicated that during heatwaves characterized by high humidity, the UHI intensity tends to remain constant or even decrease, a result that aligns with and further confirms the observations made by Kim et al. [13]. These complex and nuanced effects must be carefully considered when evaluating the thermal performance of buildings and the overall urban environment under overheating conditions.

Building upon the need for a more refined understanding of extreme heat events, Ji et al. [15] proposed a novel method for identifying extremely hot years (EHY) for a given climate. Their research highlighted a critical limitation in existing selection criteria for EHYs, which often rely solely on the duration and severity of heatwaves and tend to ignore the crucial relationship between these criteria and the potential for indoor overheating within buildings. To address this gap, their study suggested an innovative approach that utilizes the Percentage of Synchronization (POS) as a key index to assess the strength of this relationship. A high POS value indicates a greater likelihood and risk of indoor overheating during a particular year. Their methodology involved analyzing typical building models across five distinct climatic zones, based on a comprehensive comparison between two types of indices: a thermal-based index—which takes into account not only temperature but also other critical parameters such as relative humidity, wind speed, and the thermal response characteristics of individuals—and a temperature-based index, which relies primarily on dry bulb temperatures for the selection of Extremely Hot Years (EHY). In the same context, their study also included a comparative analysis of three key parameters related to heatwaves—duration, severity, and intensity—based on the POS index. The results of this study convincingly demonstrated that the thermal-based index provides a more reliable and accurate method for selecting EHYs, and further revealed that the intensity and severity of heatwaves are more significant factors in predicting indoor overheating risk than their duration alone.

The far-reaching consequences of the UHI effect also extend to the energy consumption of buildings within urban areas. Boudali Errabai et al. [16] undertook a detailed investigation to assess this impact through sophisticated building performance simulation across eight distinct microclimates within the city of Montreal, Canada. Four of these microclimates were characterized based on data collected from traditional weather stations, while the other four were derived from simulations using the Weather Research and Forecasting (WRF) model, allowing for a more nuanced representation of local climate variations. The comparison of energy consumption across these microclimates was made using the Cooling Degree Hours (CDH) index, which is defined as the cumulative sum of the temperature differences above a defined comfort threshold. The results of their energy simulations clearly demonstrated a significantly increased demand for cooling

energy in urban environments compared to surrounding rural areas, directly attributable to the higher ambient air temperatures associated with the UHI effect. Their findings also indicated that the magnitude of this increased energy demand can vary depending on the specific characteristics of the building, such as its level of thermal insulation and the nature of its immediate surroundings.

In a related but distinct approach, the study conducted by Yu et al. [17] adopted a methodology that focused on quantifying the additional number of hot days (referred to as Extra Hot Day Exposure or EHDE) directly caused by the UHI phenomenon. This was defined as the difference in the total number of hot days experienced in an urban area compared to a rural area with otherwise similar surrounding conditions. In contrast to other studies that often treat urban areas in a relatively homogeneous manner from an internal urban perspective [18–20], this research was grounded in the Local Climate Zones (LCZ) classification system developed by Stewart and Oke [21]. This classification allowed the researchers to categorize the study areas from a broader global perspective and to identify which specific types of urban zones are most vulnerable to the UHI effect. The results of their study revealed a striking finding: EHDE represents nearly half of all hot days experienced in the studied urban areas, highlighting the substantial contribution of UHI to heat exposure. Furthermore, their analysis indicated that areas with particularly high EHDE rates are often located in countries facing challenges related to poverty and a higher proportion of age-related vulnerability within their populations, underscoring the social equity dimensions of UHI impacts. These socioeconomic factors were also carefully considered in the study conducted by Nilusha et al. [22], which similarly found that surface characteristics, anthropogenic heat emissions, and population characteristics all exert a significant impact on the UHI effect. Their adopted method involved extracting Surface UHI (SUHI) information from satellite imagery, carefully distinguishing the land cover characteristics of different areas, and identifying the major factors contributing to the UHI effect at a fine-grained neighborhood scale. Finally, the relationship between these various variables and the SUHI was quantified through rigorous statistical analysis. The results of their study showed that variations in SUHI are closely related to the development patterns of agricultural and forested areas in surrounding rural zones. A key conclusion of their work was that an increase in SUHI is strongly associated with the replacement of vegetated areas by built environments, such as the development of new residential and commercial neighborhoods.

The critical role of land cover in influencing UHI was also the central focus of the investigation by Hurduc et al. [23], who specifically examined the impact of land cover typology and the temporal dimension in the calculation of SUHI. Their study collected high-resolution data from three major European cities—Paris, Madrid, and Milan—using a geostationary satellite station, which offers greater reliability compared to orbiting satellites and allows for the acquisition of SUHI data on an hourly basis. The results of their analysis showed that, for the same measured urban temperature, the SUHI can exhibit significant variations depending on the specific land cover characteristics of the surrounding rural areas. Additionally, their analysis revealed that the temporal dimension, whether considered on a seasonal or a diurnal scale, has a notable impact on the calculated SUHI value, highlighting the dynamic nature of the UHI effect.

Beyond the temporal framework and land cover characteristics, several studies have investigated other key factors influencing UHI. For example, the research conducted by Firozjaei et al. [11] specifically aimed to explore the effect of the presence of a large body of water, in this case the Caspian Sea, on SUHI. Their analysis was conducted across eleven cities located around the Caspian Sea, where SUHI was calculated for both coastal and non-coastal cities during different seasons and times of the day. The effect of the

distance from the sea on SUHI was then quantified based on several relevant parameters, including distance itself, population size, urban area extent, and biophysical properties of the surrounding landscape. The results of their study indicated that as the distance from the Caspian Sea increases, the SUHI also tends to increase, although this effect was observed to be reversed during nighttime hours, suggesting a complex interplay between proximity to water and diurnal temperature variations.

Another important aspect of UHI research is the influence of city size, which was the focus of a study by Deng et al. [24]. Their research aimed to explore how the overall size of a city impacts its SUHI. To distinguish between different types of surface cover within the studied cities, they utilized MODIS Land Cover (LC) data. The results of their analysis showed that increased city size has a negative impact on the cooling capacity provided by urban vegetation, suggesting that larger cities may experience a more pronounced UHI effect due to the limited cooling influence of green spaces. Similarly, a study conducted by Touchaei and Wang [25] evaluated the effect of urban morphology, specifically the three-dimensional structure of the city, on Urban Heat Island Intensity (UHII). Their analysis involved a detailed comparison of results obtained from four distinct neighborhoods within the city of Montreal. The modeling approach they employed included sophisticated Weather Research and Forecasting (WRF) simulations, multi-layer urban canopy models, and a Building Energy Model (BEM). Their methodology involved acquiring high-resolution aerial photographs of the study areas and extracting precise building height information from the city's comprehensive database. The BEM was then utilized to calculate energy consumption and heat emissions from buildings within the neighborhoods, while air temperature simulations were performed using the WRF model. The Sky View Factor (SVF), a measure of the amount of sky visible from a point on the ground, was determined through statistical analysis. Finally, UHII was calculated based on the simulated temperature difference between the urban neighborhoods and surrounding rural areas. The results of their analysis suggested higher air temperatures during nighttime and lower temperatures during daytime in urban areas, potentially due to latent heat flux and cloud cover. Additionally, their study concluded that changes in the Sky View Factor (SVF) had a negligible effect on UHII in their study areas. Importantly, their research also confirmed that urban morphology plays a significant role in accurately simulating regional climates.

Recognizing the significant impact of the UHI phenomenon on the quality of life and vulnerability of urban populations [11,17], several studies have emphasized the urgent need for the implementation of effective mitigation strategies to alleviate these adverse effects. Nilusha et al. [22] specifically suggested that mitigation procedures should prioritize socially disadvantaged neighborhoods, as these communities are often more vulnerable to the temperature variations and associated health risks caused by UHI. On the other hand, Zhao et al. [26] investigated the impact of the spatial connectivity of UHIs, attempting to construct a network of UHIs by identifying the major heat sources within a city and the heat transmission links between them. The results of their research showed that, in theory, corridors or pathways linking these heat nodes can contribute to the intensification of the overall UHI effect. Therefore, based on their findings, they proposed that mitigation efforts should focus on addressing disruptions within these heat corridors rather than arbitrarily adding resistance zones without a clear understanding of the underlying thermal network.

Building upon the understanding of UHI and its impacts, other studies [22,25,27–29] have proposed various urban mitigation solutions aimed at reducing UHI intensity and its negative consequences. These solutions include increasing urban vegetation and incorporating water bodies into the urban landscape, reducing anthropogenic heat emissions from sources like traffic and industrial activities, utilizing reflective materials on building roofs

and pavements to decrease solar heat absorption, and introducing the concept of cool pavements designed to have lower surface temperatures. Cortes et al. [30] and Ignacio et al. [31] have attempted to evaluate the effectiveness of these diverse mitigation strategies through detailed simulations of different urban scenarios conducted using the ENVI-met[®] software version 5.5.1, a widely used microclimate modeling tool. The results of their simulations generally showed that all these strategies can effectively contribute to reducing air temperatures within urban areas, with the scenario that combined multiple mitigation strategies often proving to be the most effective in achieving significant temperature reductions.

In another innovative approach, Zhao et al. [32] introduced a multi-level thermal environment network approach, which integrates both two-dimensional and three-dimensional urban structural parameters to identify and ultimately mitigate the formation of both urban heat islands and urban cold islands through the application of advanced simulation models. By skillfully combining spatial pattern analysis techniques, connectivity theory principles, and thermal resistance modeling, this study effectively demonstrated the potential of a strategically designed cooling network in significantly reducing high-temperature zones within a city and offered valuable insights for the development of sustainable and effective urban climate adaptation strategies.

Despite the significant advancements in our understanding of the UHI phenomenon through the numerous existing studies, there remains a persistent need to develop a more comprehensive and integrated understanding of the specific parameters that interact with UHIs and their complex synergistic effects with other climate events, particularly heatwaves. Key unanswered research questions persist, such as: how do specific urban characteristics like urban density, the extent and distribution of vegetation, and demographic distribution patterns directly affect the intensity of the UHI effect? Furthermore, to what extent can various commonly used thermal comfort indices be considered reliable and accurate tools for assessing and quantifying UHI intensity across different urban contexts? Addressing these critical research questions and filling these existing knowledge gaps can significantly help guide future studies aimed at achieving a more complete understanding of the Urban Heat Island effect and developing more effective and targeted mitigation strategies, ultimately contributing to the creation of more sustainable and resilient urban environments for the future.

In the specific context of Canada, and unlike many other major urban centers globally, the city of Montreal has, to date, not been the subject of sufficiently in-depth and comprehensive research specifically focused on thoroughly investigating the full extent of its Urban Heat Island and the specific effects it has on its diverse local populations. While various local initiatives and efforts have been undertaken to address this growing phenomenon, the absence of a comprehensive and detailed study of localized thermal data significantly limits the ability of urban planners and policymakers to implement truly targeted and effective mitigation solutions and long-term strategies tailored to Montreal's unique urban characteristics and climate.

Therefore, this study directly focuses on meticulously analyzing the readily available thermal landscape data specifically for the city of Montreal to directly address and fill this critical knowledge gap. The overarching aim of this research is to gain a deeper understanding of the specific factors that contribute to the intensification of UHIs within Montreal's urban areas and to comprehensively assess the extent and spatial distribution of their impact on the city's diverse urban fabric and its population. By providing a detailed analysis of Montreal's UHI characteristics, this study intends to contribute valuable insights that can directly inform the development and implementation of more effective and locally relevant urban planning strategies ultimately aimed at alleviating the adverse impacts of

urban heat islands on public health and enhancing the overall sustainability and resilience of the city.

2. Materials and Methods

2.1. Methodology

Montreal, the largest city in Quebec and the second largest in Canada, is a major urban center located on an island in the St. Lawrence River. With a population of 1,762,949 inhabitants according to the 2021 census, this urban center is divided into 19 boroughs, presenting a great diversity of urban landscapes and demographic dynamics. This diversity makes Montreal an ideal setting for studying heat island phenomena. Figure 1 illustrates a flowchart of a methodical multi-step approach we have followed in this study to analyze the UHI effect on the Island of Montreal.

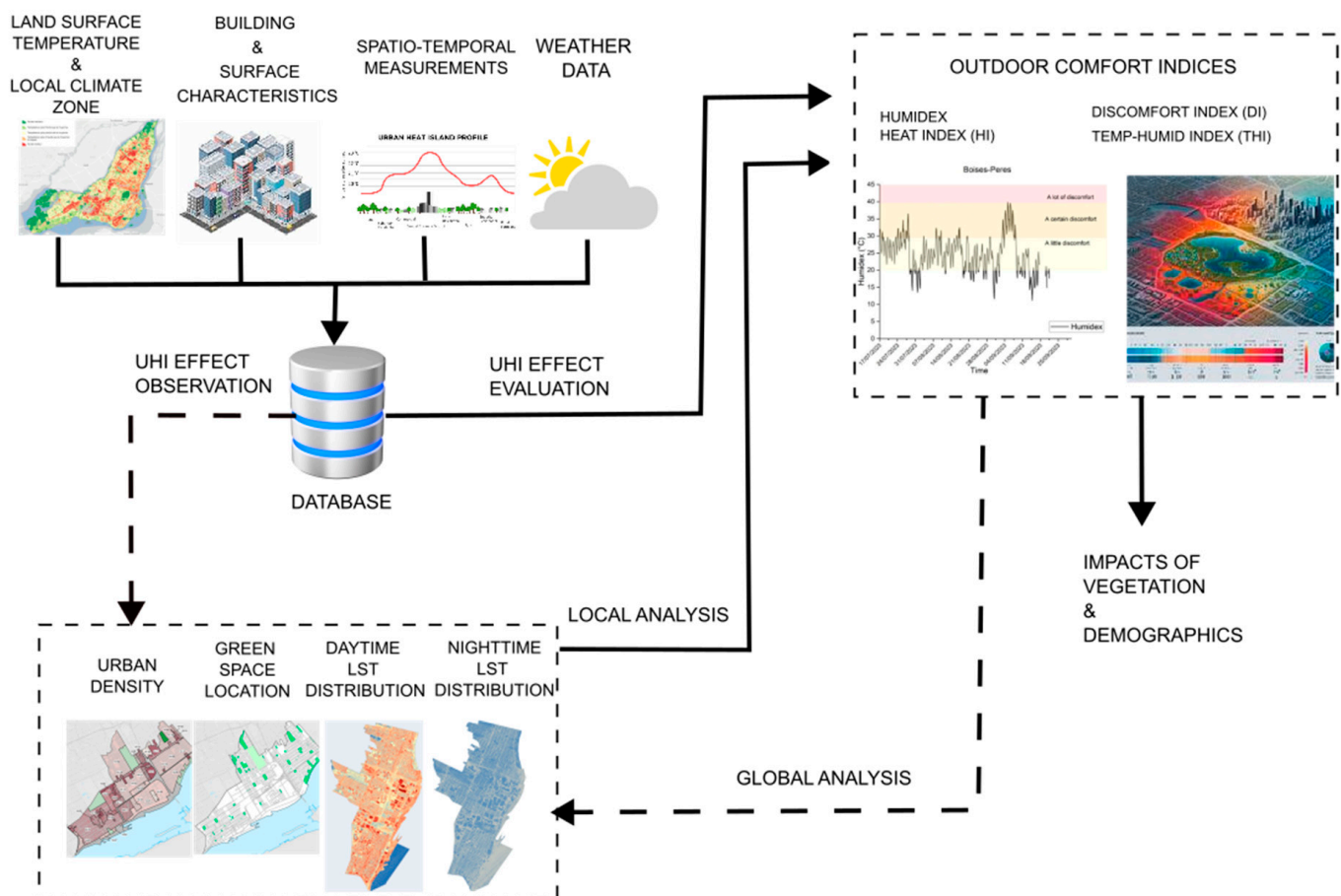


Figure 1. Flowchart of the proposed methodology.

First, a preliminary analysis was conducted to gain an overview of the island's environmental and urban characteristics. This step included exploring areas of heat and cool island concentration using satellite images. Next, the collected data, including air temperature, relative humidity, and dew point measurements, were processed to further analyze microclimates. This processing involved removing erroneous data, creating average values, and selecting the appropriate study period based on data availability and quality. Then, comfort indices were determined based on the processed data. These indices, based on empirical equations and thresholds (cf. Appendix A), help better understand the thermal sensations of the population [33–37]. Once the indices were estimated, the results were analyzed to identify the factors influencing heat islands and quantify their effects. Finally,

conclusions were drawn from the results, along with recommendations for urban planning strategies to reduce heat islands. These suggestions aim to improve the thermal comfort of residents and mitigate the effects of heatwaves on the Island of Montreal.

2.2. Data Collection

The thermal data used for this study were provided by the City of Montreal as publicly available open data [29]. We have linked two types of data: surface thermographic data derived from satellite and airborne images, and air climate data collected from sensors. Data generated by the 15 currently installed stations were used. The 15 sensors installed are distributed across the Island of Montreal. Figure 2 shows the location of the sensors based on the coordinates provided by the City of Montreal. Table 1 below shows the location of each sensor according to the administrative boundaries of the city.

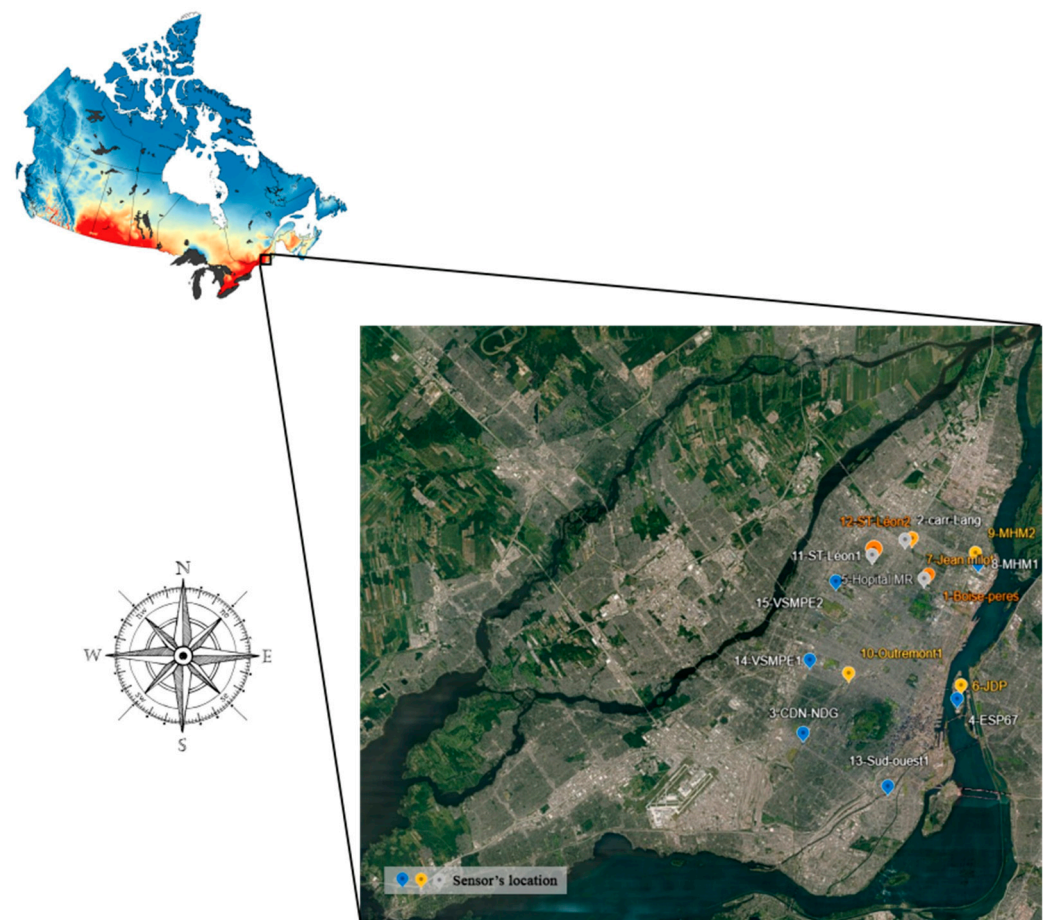


Figure 2. Studied area (The red color indicates the peak intensity of the UHI effect).

Atmospheric correction and temperature calculations integrate an emissivity map derived from the NDVI (Normalized Difference Vegetation Index) and has a maximum error margin of 2 °C. A major advantage of this method is the improvement of the initial thermal resolution from 100 m to 30 m through resampling based on Landsat multispectral data [29]. It should be noted that sometimes the available satellite images do not meet the selection criteria. In 2023, the only image meeting the conditions was captured during a heatwave, explaining the temporary increase in the heat island phenomenon.

Concerning airborne images, the city performed territorial mapping through thermal infrared images including 32 spectral bands, taken during both day and night, with respective resolutions of 2 m and 1 m. The overflights occurred during specific time slots: between

12 p.m. and 3 p.m., when inert materials reach their peak temperature, and between 12 a.m. and 4 a.m., when temperatures are at their minimum before sunrise. The images were geometrically corrected to eliminate distortions due to linear scanning and atmospheric disturbances. Orthorectification was performed using the city of Montreal's Digital Surface Model (DSM) produced from airborne LiDAR data. The data were then calibrated into luminance units and converted into surface temperatures using atmospheric corrections (via the MODTRAN code) and a TES (Temperature-Emissivity Separation) algorithm.

Table 1. Location of measurement stations and sensor coordinates.

Station's Name	Geographical Location	Sensor Coordinates	
		Longitude	Latitude
1-Boise-Peres	Rosemont-La Petite-Patrie	−73.556306	45.57569
2-Carref_Langelier	Saint-Léonard	−73.573583	45.59319
3-CDN-NDG-1	Côte-des-Neiges-Notre-Dame-de-Grâce	−73.648944	45.49355
4-Espace_67	Ville-Marie	−73.535417	45.51102
5-Hopital_M-R	Rosemont-La Petite-Patrie	−73.559639	45.57333
6-Jean-Drapeau_Etang	Ville-Marie	−73.532472	45.51802
7-Jean-Milot	Mercier-Hochelaga-Maisonneuve	−73.568444	45.59394
8-MHM 1	Mercier-Hochelaga-Maisonneuve	−73.519722	45.58097
9-MHM 2	Mercier-Hochelaga-Maisonneuve	−73.521556	45.58633
10-Outremont 1	Outremont	−73.615361	45.52438
11-Saint-Léonard 1	Saint-Léonard	−73.597917	45.58536
12-Saint-Léonard 2	Saint-Léonard	−73.596472	45.58630
13-Sud-Ouest-1	Le Sud-Ouest	−73.586583	45.46594
14-VSMPE 1	Villeray-Saint-Michel-Parc-Extension	−73.644056	45.53125
15-VSMPE 2	Villeray-Saint-Michel-Parc-Extension	−73.624667	45.57175



Field checks were conducted to validate and calibrate the thermographies. This involved installing 30 thermal sensors of the “iButton” type and 11 beacons (white-painted surfaces or 3 m × 3 m Tyvek panels) on various types of soil and on the roofs of some buildings. Complementary measurements were also taken using infrared guns [38,39]. Other data specifications are summarized in Table 2.

Table 2. Data specifications.

Specifications	Values
Acquisition period	3 August to 3 September 2016
Wind direction	130°
Average wind speed	16 km/h
Average air temperature on 20 August 2016	28.9 °C
Thermal sensor	TASI 600 (8–12 µm)
Image resolution	2 m/pixel
Planimetric accuracy of thermography	±2.3 m
Thermal measurement accuracy	±3 °C

Climate data were generated and recorded by Hobo Micro stations equipped with integrated solar panels (RX2102) and Smart Sensors (S-THB-M002) (from HOBO MicroRX Station series, manufactured by Onset Computer Corporation, based in Bourne, MA, USA) for measuring relative humidity and air temperature. The sensors were installed at a height of three meters in open areas, free from any buildings. The collected data were recorded in real time and transmitted via a cellular network to a centralized database. The sites were selected based on several criteria, including heatwave episodes, potential for heat island reduction projects, and high rates of mineralized surfaces [9]. The characteristics of the measurement instruments used in this process are listed below in Table 3.

Table 3. Characteristics of measuring instruments.

Instrument	Image	Operating Range	Accuracy	Objective
Onset HOBO MICRO (RX2102)		−4 to 140 °F (−20 to 60 °C)	±8 s per month in 32 to 104 °F (0 to 40 °C) range ±30 s per month in −40 to 140 °F (−40 to 60 °C) range	Saving obtained data
Smart Sensors (S-THB-M002)		−40 °C to 75 °C (−40 °F to 167 °F)	±0.21 °C from 0° to 50 °C (±0.38 °F from 32 to 122 °F)	Measuring relative humidity and air temperature

3. Spatial Patterns of UHI-Contributing Factors: Human Thermal Exposure and Discomfort

According to the satellite image from 6 July 2023, which represents the heat islands presented in Figure 3a, an uneven distribution of cool islands and heat islands is observed across the Island of Montreal. Cool islands are primarily concentrated in the northeastern and western parts of the island, areas characterized by denser vegetation and lower urbanization. In contrast, heat islands are concentrated in the downtown area, the Saint-Laurent area, and the southern coast of Montreal, regions marked by high urban density and reduced vegetation coverage.

These spatial disparities highlight the impact of urban planning on local temperatures. Highly urbanized areas absorb more solar radiation due to impermeable materials, such as asphalt and concrete, leading to a significant increase in surface temperatures. In contrast, green spaces and less developed areas play a key role in reducing temperatures, as correlated in Figure 3b.

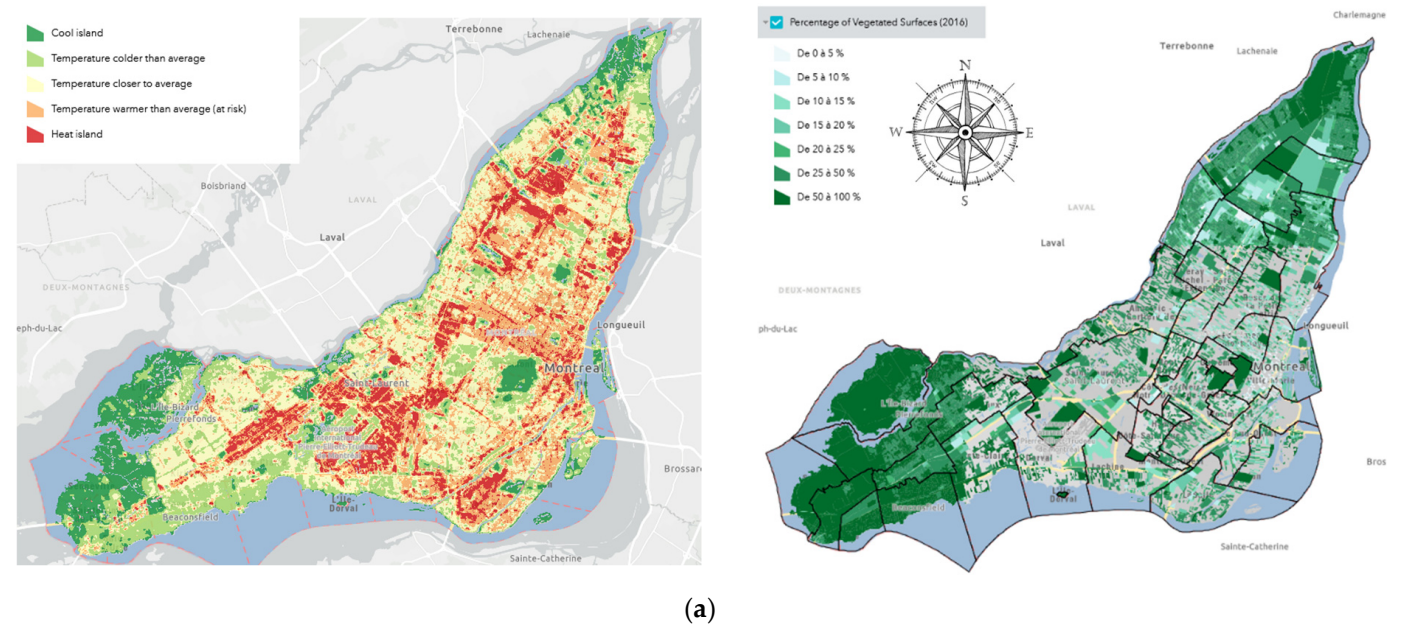


Figure 3. Cont.

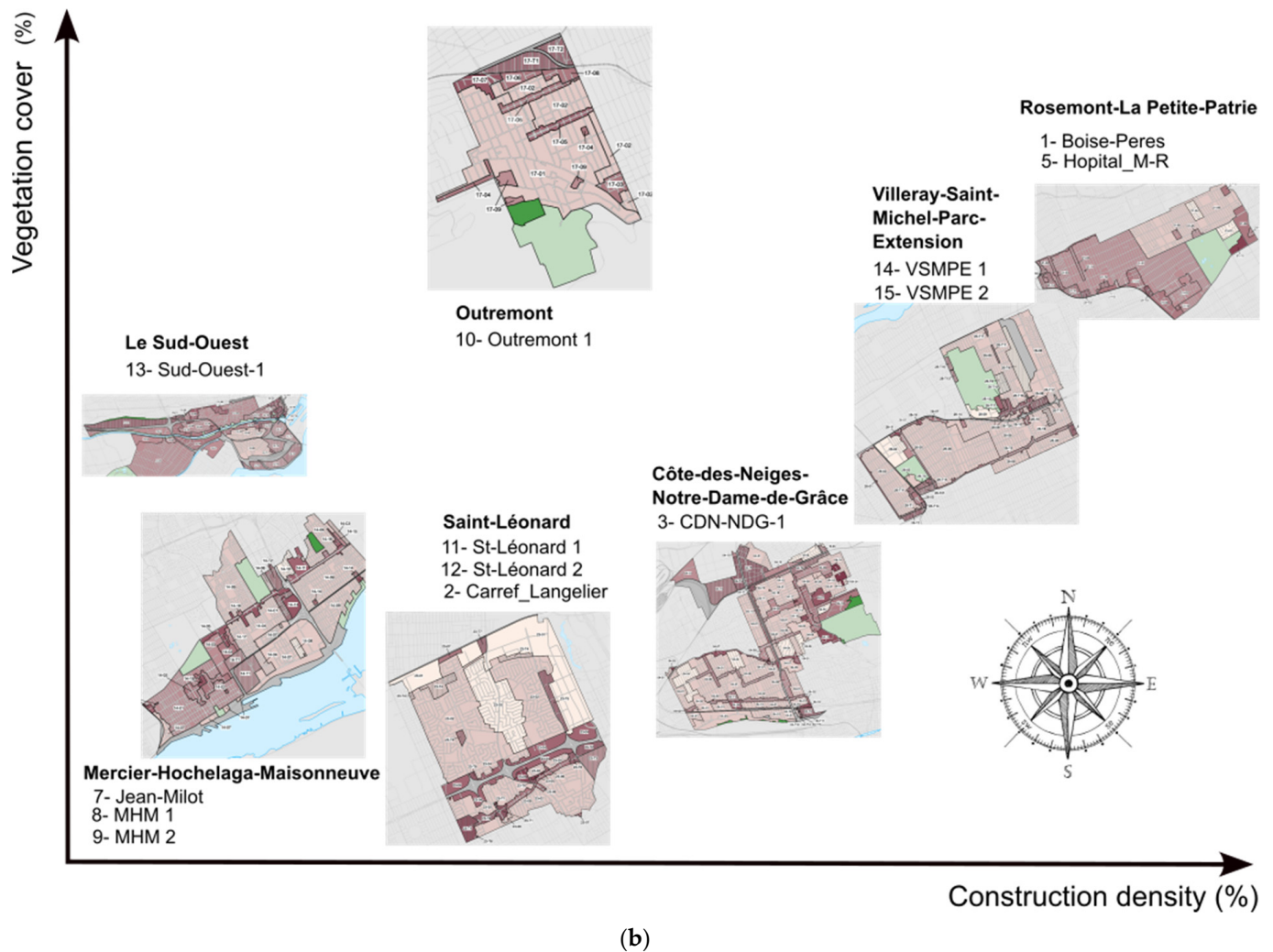


Figure 3. Satellite image taken on 6 July 2023 [39] (a), and vegetation cover versus urban density [40] (b).

To better understand the causes of this distribution and identify the factors that influence these phenomena, a comparative analysis between the different areas of the Island of Montreal is necessary (cf. Appendix B). Demographically, there is a significant variation between the different areas of the island. According to the 2021 census, Côte-des-Neiges–Notre-Dame-de-Grâce has the largest population (170,583 inhabitants), followed by Villeray–Saint-Michel–Parc-Extension (145,090 inhabitants), Rosemont–La Petite-Patrie (141,813 inhabitants), Mercier–Hochelaga–Maisonneuve (140,627 inhabitants), and Ahuntsic–Cartierville (135,336 inhabitants).

It is also noted that the Plateau–Mont-Royal borough has a very high population density (13,015 inhabitants/km²) compared to other boroughs, followed by the Rosemont–La Petite-Patrie borough (8947 inhabitants/km²). This variation in demographic distribution can directly influence the intensity of heat islands.

Figure 4 compares the main boroughs of the City of Montreal in terms of urban density, green surface area, and daytime and nighttime surface temperature distributions.

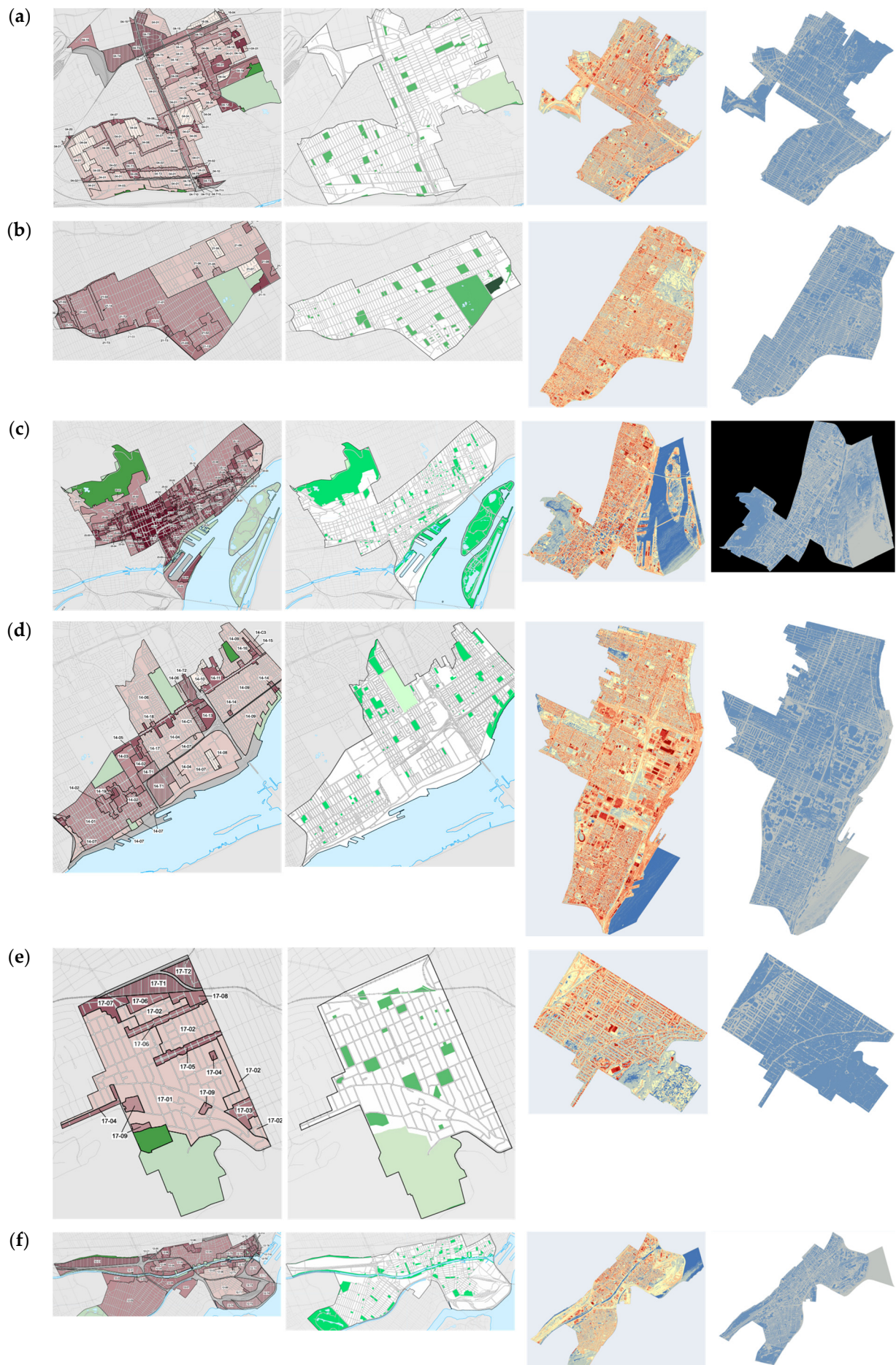


Figure 4. Cont.

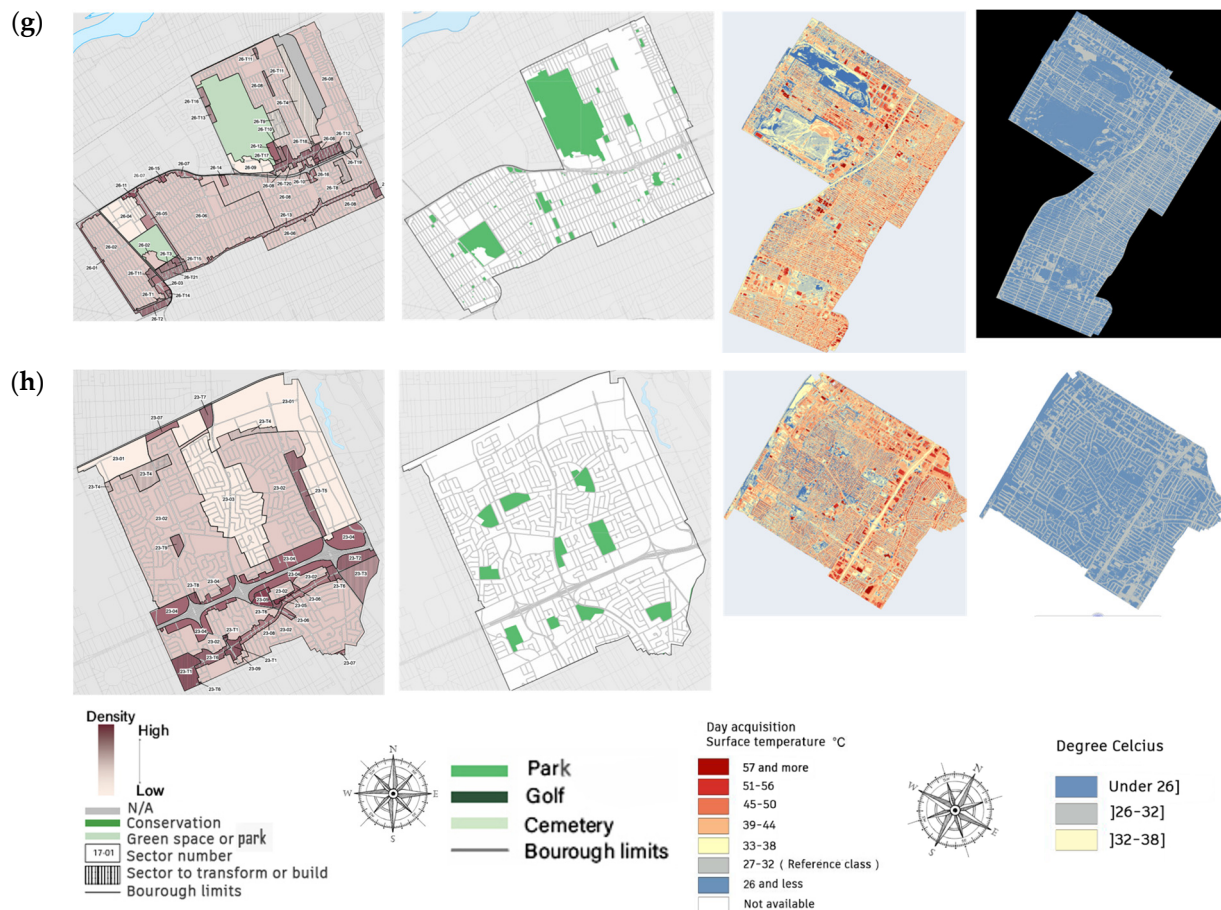


Figure 4. Urban density, green space location and daytime and nighttime surface temperature distributions for (a) Côte-des-Neiges–Notre-Dame-de-Grâce, (b) Rosemont–La Petite-Patrie, (c) Ville-Marie, (d) Mercier–Hochelaga–Maisonnette, (e) Outremont, (f) Sud-Ouest, (g) Villeray–Saint-Michel–Parc-Extension, (h) Saint-Léonard [40–43].

According to Figure 4a, the urban density map of the Côte-des-Neiges–Notre-Dame-de-Grâce borough, characterized by a population of 170,583 inhabitants and a density of 7956 inhabitants/km², shows a fairly high density mainly in the northern and northwestern parts. This variation may be due to urban zoning regulations and urban sprawl, which becomes less dense as one moves away from the city center.

The map of parks and green spaces shows an equitable distribution of parks in this borough. The area of parks accounts for 3.6% of the total area of the borough, while the area of green spaces rises to 9.88%, including the large cemetery. The area dedicated to parks and green spaces is very limited, especially for the most populous borough in the region.

According to the airborne image of the borough, over the course of the day, it is observed that the surfaces with the highest temperatures are open sports fields, followed by the roofs of buildings. The temperatures in the parks and the large cemetery remain relatively low.

During the night, it is observed that the surface temperature drops below 26 °C for the majority of surfaces. In contrast, the temperature of the pavement remains in the range of 26 °C to 32 °C. This can be explained by the thermal properties of the asphalt used for road construction. It absorbs a large amount of solar radiation rather than reflecting it during the day due to its dark color and very low albedo. The stored heat is slowly released during the night, which contributes to maintaining high nocturnal temperatures.

Figure 4b shows meaningful maps concerning Rosemont–La Petite-Patrie. This borough is characterized by a population of 141,813 inhabitants and a density of 8947 inhabitants/km².

According to the urban density map, a fairly low density is observed in the northern part of the borough, with a medium density spread across the rest of the area.

The map of parks and green spaces shows an inequitable distribution of parks in this borough, especially in the west, where there is a lack of parks. The area of parks accounts for 15.24% of the total area of the borough. Overall, the area dedicated to parks and green spaces is relatively low for such a density, with the denser western part showing a lack of parks and green spaces.

According to the airborne image of the Rosemont–La Petite-Patrie borough, it is observed that the surfaces with the highest temperatures, exceeding 51 °C, are open sports fields, roofs of certain secondary schools, shopping centers, and the STM transport center. Temperatures in the parks and green spaces remain below 38 °C. During the night, it is observed that the surface temperature drops below 26 °C for most surfaces. In contrast, the temperature of the pavement remains in the range of 26 °C to 32 °C. The thermal characteristics of asphalt offer a plausible explanation for this phenomenon.

Ville-Marie presents a unique geographical case which is characterized by a population of 104,944 inhabitants and a density of 6353 inhabitants/km². According to the urban density map (Figure 4c), a very high density is observed in the western part and a medium density in the rest of the borough. This variation may be due to historical reasons, as this area includes the current downtown and the former city center.

The map of parks and green spaces shows an unequal distribution of green spaces. This borough includes part of the Mount Royal hill and the two islands, Sainte-Hélène and Notre Dame. Table 4 presents the distributed vegetation and water cover percentages for the two islands.

Table 4. Vegetation and water body covers of Sainte-Hélène and Notre Dame islands.

Ville Marie	Whole Borough	Coastal City	Sainte-Hélène Island	Notre Dame Island
Vegetation cover (%)	24.39	17.77	70.54	47.26
Water body cover (%)	-	-	6.86	32.89

From the airborne image of the Ville-Marie borough, surfaces with the highest temperatures, which can exceed 51 °C, include open sports fields, roofs of certain secondary schools, shopping centers, and the roofs of quay constructions. Temperature in parks and green spaces remains lower, below 38 °C.

The Mercier–Hochelaga–Maisonnette borough is characterized by a population of 140,627 inhabitants and a density of 5534 inhabitants/km². According to the urban density map (Figure 4d), a higher density is observed in the southern part compared to the rest of the borough. The map of parks and green spaces shows an inequitable distribution of parks in this borough, especially in the south and southeast, where there is a lack of parks. The area of parks accounts for 5.4% of the total area of the borough. The area of parks and green spaces rises to 8.27% when including the large cemetery. Overall, the area dedicated to parks and green spaces is very low for such a density.

According to the airborne image of the Mercier–Hochelaga–Maisonnette borough, it is observed that the surfaces with the highest temperatures, which can exceed 51 °C, include open sports fields, large retail roofs, and warehouses. Temperatures in the parks and green spaces remain below 38 °C.

The boroughs of Outremont and Sud-Ouest are characterized by a population of 24,629 inhabitants and a density of 6397 inhabitants/km², 84,553 inhabitants and a density of 5392 inhabitants/km², respectively. A higher density is observed in the northern part compared to the rest of the borough (Figure 4e). The map of parks and green spaces shows

an equitable distribution of parks in these boroughs. The area of parks accounts for 5.98% of the total area of these boroughs, and rises to 24.5% when including the large cemetery.

According to the airborne image of the Outremont and Sud-Ouest boroughs, it is observed that the surfaces with the highest temperatures, which can exceed 51 °C, are the roofs of houses and open sports fields. Temperatures in parks and green spaces remain below 38 °C. During the night, it is observed that the surface temperature drops below 26 °C for most surfaces. In contrast, the temperature of the pavement remains in the range of 26 °C to 32 °C.

The Villeray–Saint-Michel–Parc-Extension borough is characterized by a population of 145,090 inhabitants and a density of 8799 inhabitants/km². A low density is observed across most of the area, with high concentration in the center and the west. The map of parks and green spaces shows an unequal distribution of parks in this borough, with the majority of the park area concentrated in two regions (Parc Jarry to the south and Parc Frédéric-Back to the northwest). The total area of parks accounts for 14.66% of the total area of the borough. Overall, the area dedicated to parks and green spaces is very low for such a density.

The borough of Saint-Léonard is characterized by a population of 79,495 inhabitants and a density of 5893 inhabitants/km². According to the urban density map (Figure 4h), a low or medium density is observed across most of the area, with a high-density band along the sides of Autoroute 40. The map of parks and green spaces shows an equitable distribution of parks in this borough. The area of parks accounts for 5.05% of the total area of the borough.

The analysis of the data generated by this sensor allowed us to establish the following graphs presenting the chosen comfort indices, as illustrated in Figure 5. The study period selected is from 17 July 2023 to 30 September 2023, covering most of the summer season.

The considered comfort indices are humidex, discomfort index (*DI*), heat index (*HI*), and temperature–humidity index (*THI*).

According to [34], humidex can be estimated by Equation (1), as follow:

$$\text{Humidex} = T + h \quad (1)$$

where: *T* is the air temperature;

$$h = 0.5555(e - 10);$$

e is the vapor pressure (hPa), calculated as follows: $e = 6.11 \times \exp\left[\frac{5417.7530}{T_{\text{dew point}}}\right]$; and $T_{\text{dew point}}$ is the dew point temperature.

Values from 20 to 29 correspond to a little discomfort; from 30 to 39, some discomfort; from 40 to 45, a lot of discomfort: avoid effort; above 45, a risky situation with possible heat stroke [34].

DI can be calculated from Equation (2) [13]:

$$DI = 0.5(T_w + T) \quad (2)$$

where: T_w is the wet-bulb temperature.

For values under 22, no heat stress is encountered; 22–24, most people feel a mild sensation of heat; 24–28, the heat load is moderately heavy, people feel very hot, and physical work may be performed with some difficulties; and above 28, the heat load is considered severe, and people engaged in physical work are at increased risk for heat illness [36]

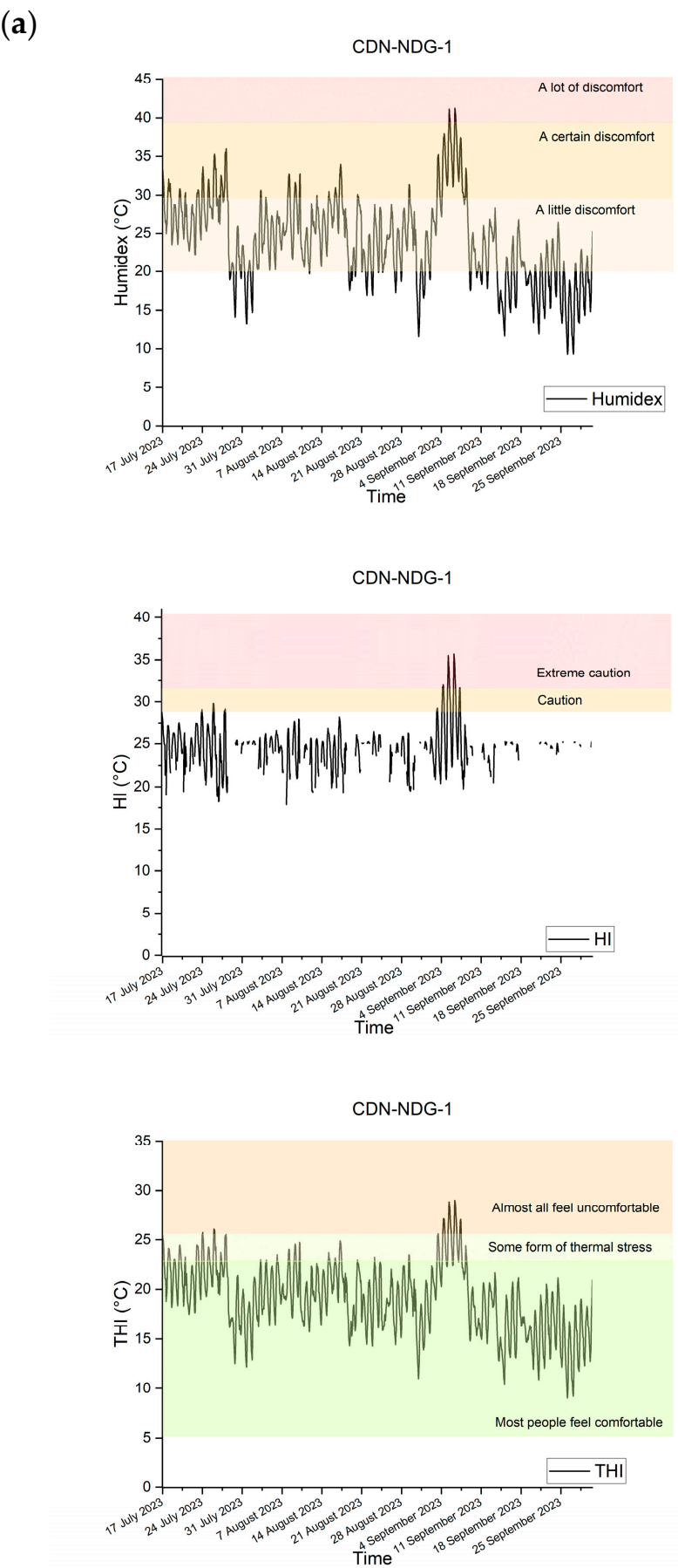


Figure 5. Cont.

(b)

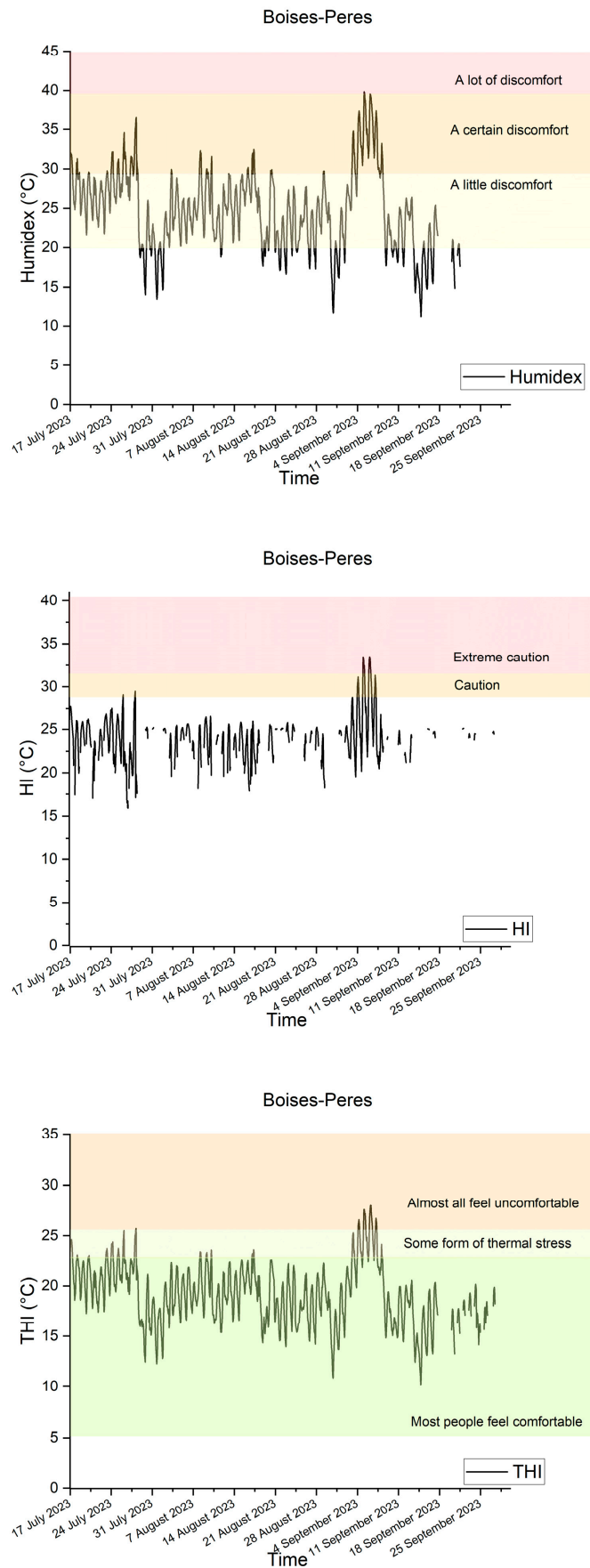


Figure 5. Cont.

(c)

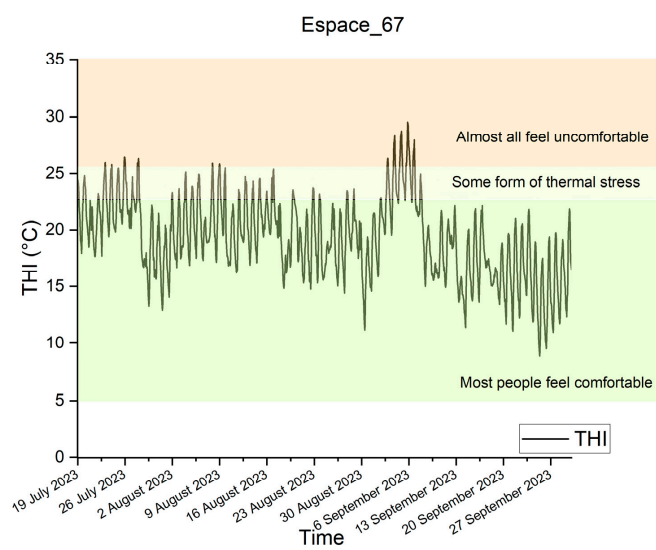
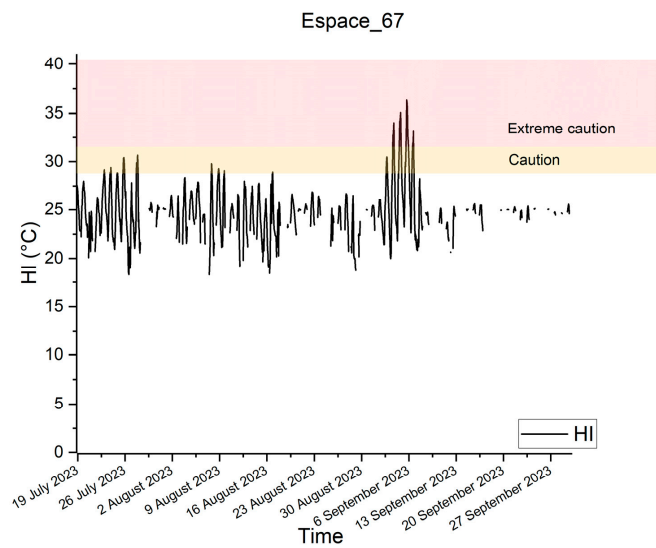
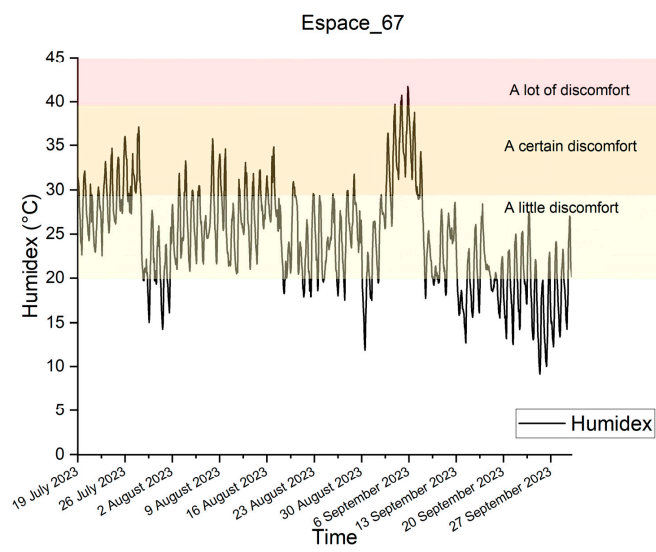


Figure 5. Cont.

(d)

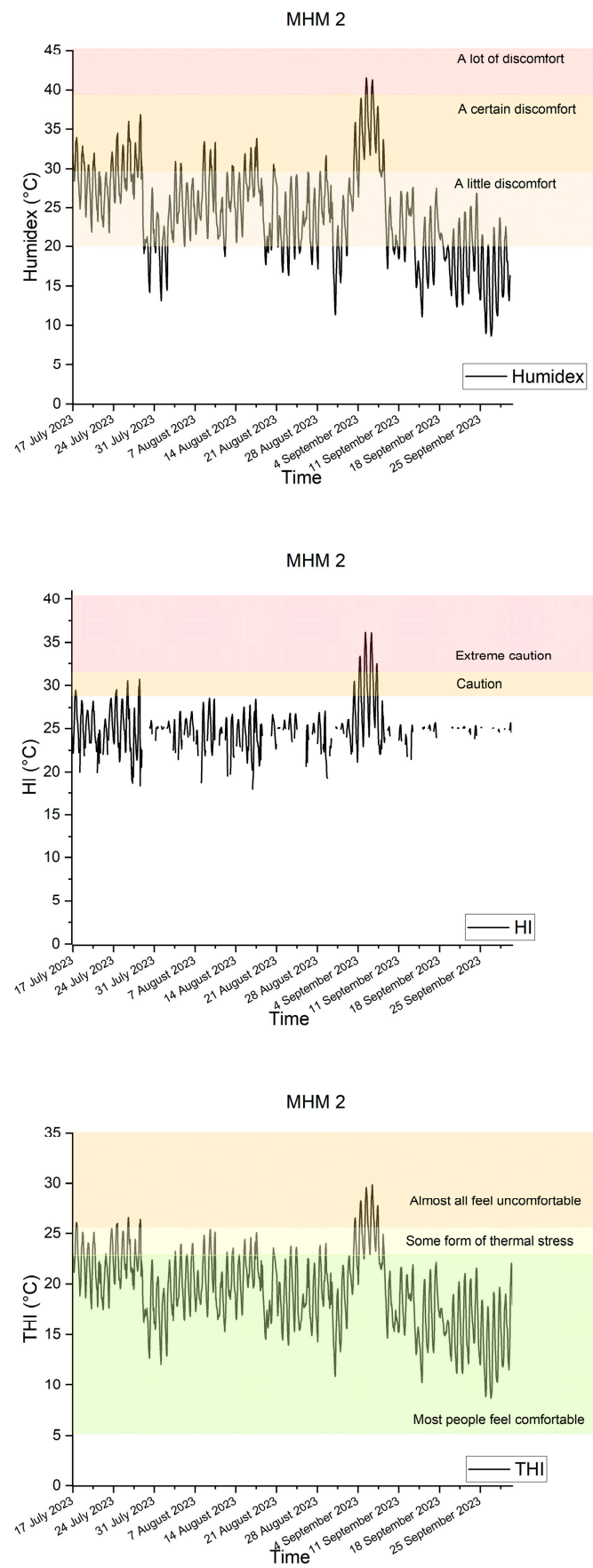


Figure 5. Cont.

(e)

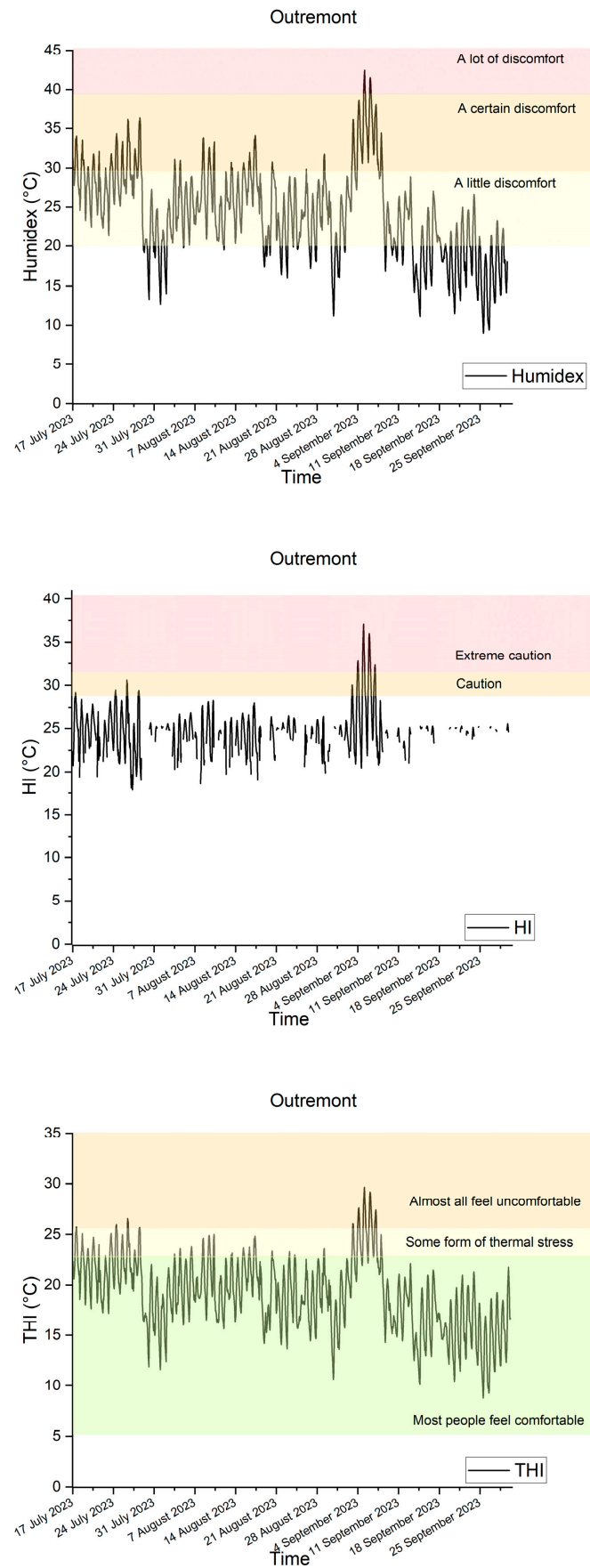


Figure 5. Cont.

(f)

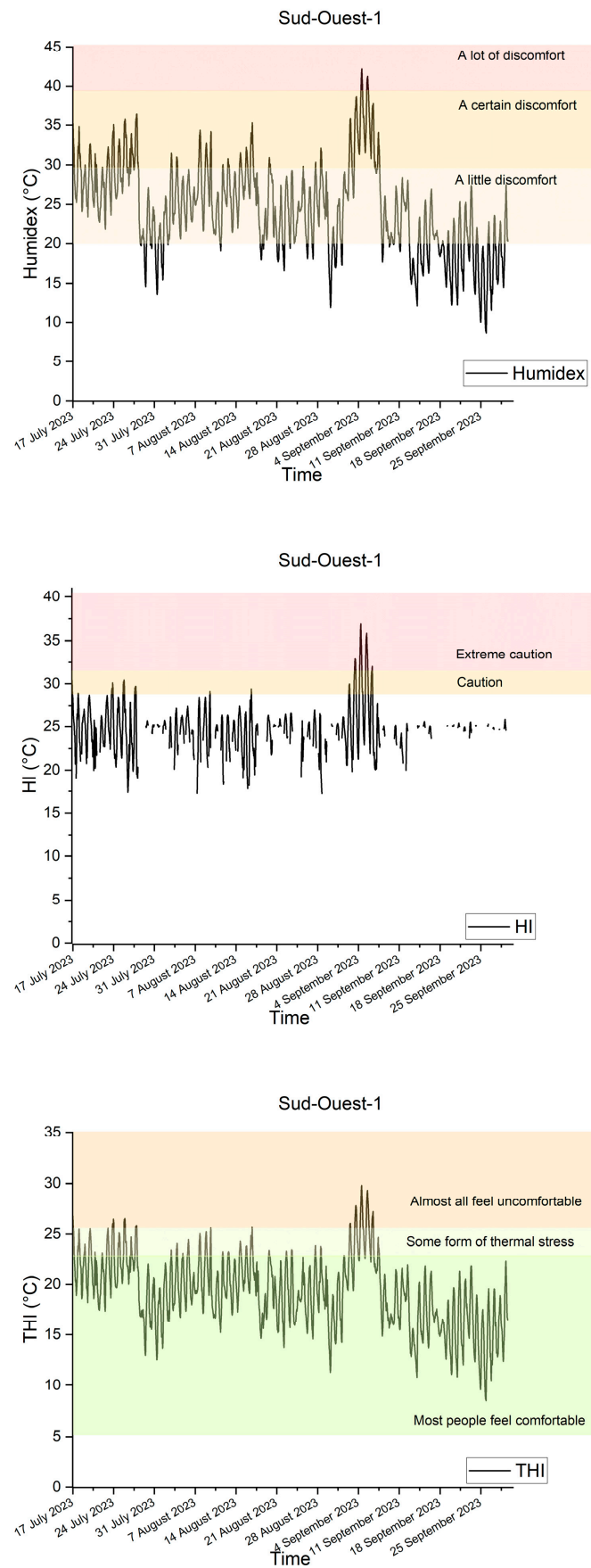


Figure 5. Cont.

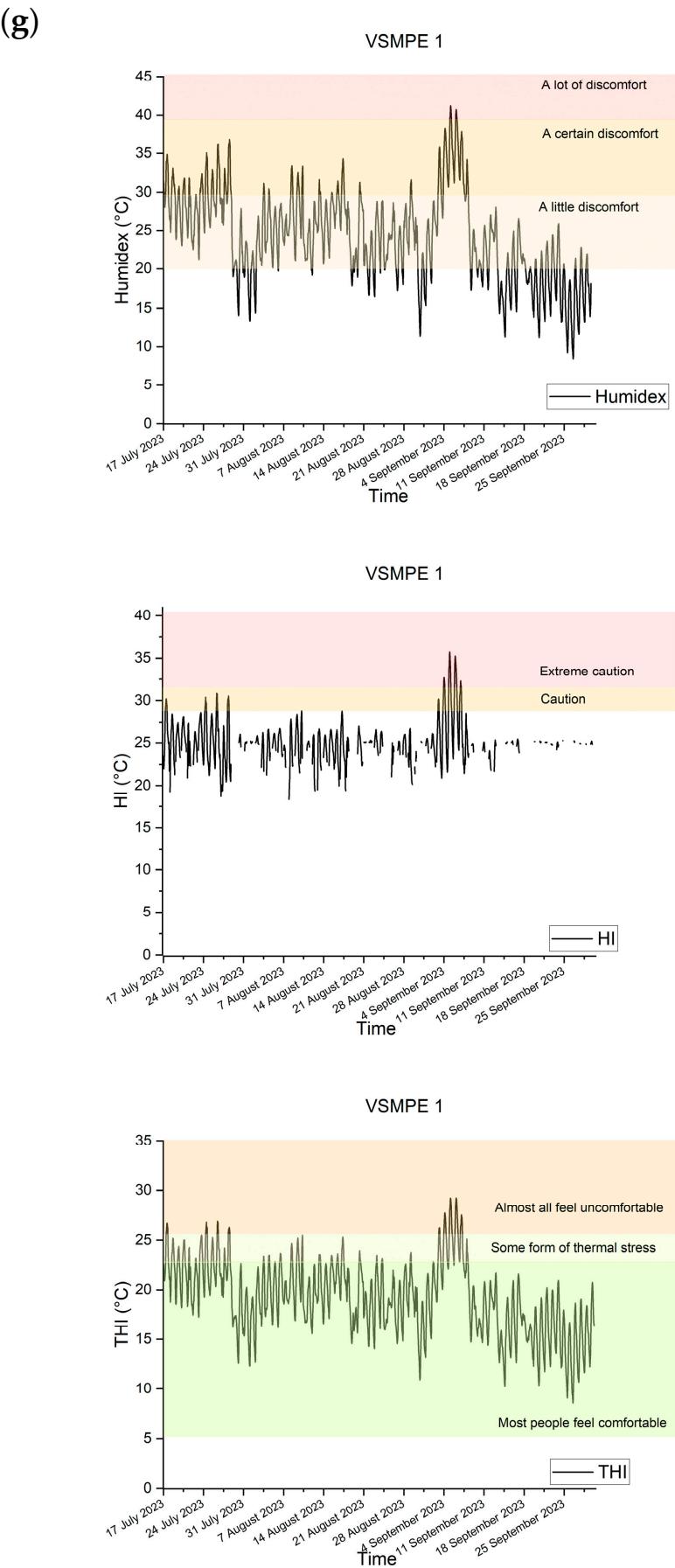


Figure 5. Cont.

(h)

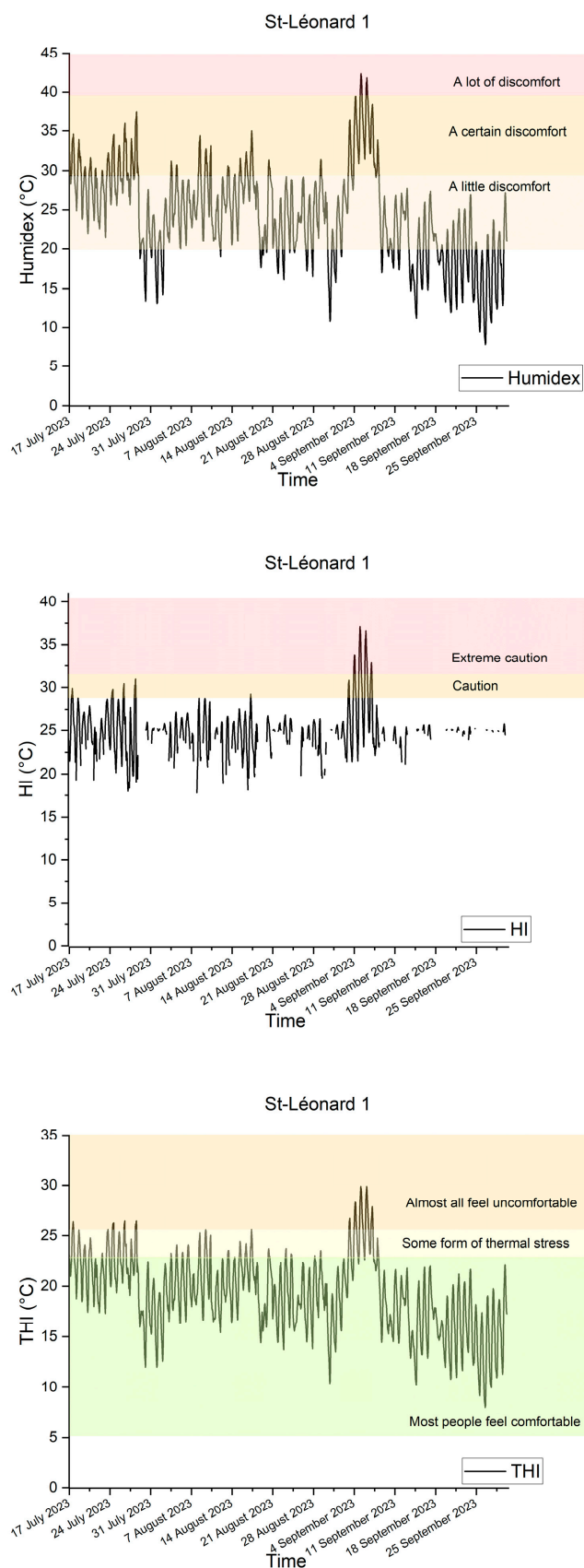


Figure 5. Outdoor thermal comfort indices for (a) Côte-des-Neiges–Notre-Dame-de-Grâce, (b) Rosemont–La Petite-Patrie, (c) Ville-Marie, (d) Mercier–Hochelaga–Maisonneuve, (e) Outremont, (f) Sud-Ouest, (g) Villeray–Saint-Michel–Parc-Extension, (h) Saint-Léonard.

Concerning *HI*, Equation (3) gives an empirical formula according to [13]:

$$HI = -8.7847 + 1.611 T + 2.338 RH - 0.1461 T RH - 1.2308 \cdot 10^{-2} T^2 - 1.6425 \cdot 10^{-2} RH^2 + 2.2117 \cdot 10^{-3} T^2 RH + 7.2546 \cdot 10^{-4} T RH^2 - 3.5820 \cdot 10^{-6} T^2 RH^2 \quad (3)$$

where: *RH* is the relative humidity (%)

The thresholds of *DI* [35] are:

27–32: Caution; fatigue possible with prolonged exposure and/or physical activity;

32–41: Extreme caution; sunstroke, muscle cramps, and/or heat exhaustion possible with prolonged exposure and/or physical activity;

41–54: Danger; Sunstroke, muscle cramps, and/or heat exhaustion likely. Heatstroke possible with prolonged exposure and/or physical activity;

≥54 Extreme danger; Heat stroke or sunstroke likely.

THI index helps determine the effect of relative humidity and air temperature on thermal comfort.

THI of about 21 °C is associated with most people feeling comfortable; at a *THI* of about 24 °C, around half of the population experiences some form of thermal stress; when *THI* reaches 26 °C, almost all feel uncomfortable [37]. Its formula is given in Equation (4), as follow:

$$THI = 0.8T + 0.2t \times \left(\frac{RH}{100} \right) \quad (4)$$

Figure 5a shows that most of the time the population experiences a little discomfort in the Côte-des-Neiges–Notre-Dame-de-Grâce borough. Several heat spikes occurred, causing a certain level of discomfort. However, most of the time, the population does not experience thermal stress. Over the heatwave period, from 4 September to 8 September, where the sensor 3-CDN-NDG-1 was located in a residential area, the temperature rose to 31.7 °C, causing significant discomfort with a maximum humidex value of 41.23 °C. The thermal load was considered severe. People engaged in physical work were at an increased risk of heat-related illnesses. Some heat spikes occurred, causing a possible risk of fatigue in cases of prolonged exposure and/or physical activity. There was an extreme risk of sunstroke, muscle cramps, and/or heat exhaustion with prolonged exposure and/or physical activity. Almost everyone felt uncomfortable, with a maximum *THI* value of 29.02 °C.

Concerning Rosemont–La-Petite-Patrie, the sensors 1-Boise-peres and 5-Hopital_MR are located in the Bois-des-Pères park and in front of the Maisonneuve–Rosemont hospital, respectively. The analysis of the data generated by the first sensor allowed us to evaluate the chosen comfort indices and presented in Figure 5b.

It is observed that most of the time, the population experienced a little discomfort. Several heat spikes occurred, causing some level of discomfort. During the heatwave from September 4 to September 8, the population near the Hopital_MR station experienced a lot of discomfort, with a maximum humidex value of 42.32 °C, whereas the humidex at the Boises-Peres station did not exceed 39.84 °C.

In addition, most of the time, the population did not experience thermal stress. However, during the heatwave, almost everyone felt uncomfortable, with a maximum *THI* value of 27.98 °C for Boises-Peres.

The sensors 4-ESP67 and 6-JDP are both located on Sainte-Hélène Island, in an esplanade and a green space belonging to Ville-Marie borough, respectively (Figure 5c). It is observed that most of the time, the population experienced a little discomfort. Several heat spikes occurred, causing some discomfort.

During the heatwave from 4 September to 8 September, the population near the Espace_67 station experienced a lot of discomfort, with a maximum humidex value of 41.73 °C, while the humidex at the Jean-Drapeau_Etang station did not exceed 39.47 °C

(not presented here). It is observed that most of the time, the population did not experience thermal stress. During the heatwave from September 4 to September 8, there was an extreme risk of sunstroke, muscle cramps, and/or heat exhaustion with prolonged exposure and/or physical activity. This effect was more pronounced in the Espace_67 region, with a maximum THI value of 27.43 °C for Jean-Drapeau_Etang and 29.56 °C for Espace_67.

The sensors 7-Jean Milot, 8-MHM1, and 9-MHM2 are located in Boisé Jean-Milot Park in the southern part of the Mercier–Hochelaga–Maisonnette borough, in a neighborhood park and in a parking lot, respectively (Figure 5d). During the heatwave from 4 September to 8 September, populations in the three regions experienced a lot of discomfort, with maximum humidex values of 41.51 °C for MHM2. Almost everyone felt uncomfortable, with maximum HI values of 29.87 °C for MHM2.

The sensor 10-Outremont is located in Pierre-Dansereau Park, in front of a residential complex in the northwest of the borough of Outremont (Figure 5e). During the heatwave from 4 September to 8 September, the temperature rose to 33.65 °C, causing a lot of discomfort with a maximum humidex value of 42.45 °C, and almost everyone felt uncomfortable, with a maximum THI value of 29.69 °C.

The sensor 13-Sud-Ouest1 is located in Cabot Square Park in an industrial area of the Sud-Ouest borough (Figure 5f). Several heat spikes occurred, causing a certain discomfort, with two peaks during the heatwave from 4 September to 8 September, reaching 32.95 °C, causing a lot of discomfort, with a maximum humidex value of 42.21 °C and a maximum THI value of 29.82 °C.

The sensors 14-VSMPE1 and 15-VSMPE2 are located, respectively, in the south and north of the borough of Villeray–Saint-Michel–Parc-Extension, in a residential area. Figure 5g shows that most of the time, the population experiences a little discomfort. During the heatwave from 4 September to 8 September, the population near the two stations experienced a lot of discomfort, with maximum humidex values of 41.21 °C and a maximum THI value of 29.25 °C for VSMPE1.

The sensors 11-ST-Léon1 and 12-ST-Léon2 are located, respectively, in a parking lot and in a park in the same area. According to the Figure 5h, it is observed that between 4 September to 8 September, populations in the three regions experienced a lot of discomfort, with maximum humidex values of 42.36 °C for St-Léonard1, and a maximum THI value of 29.90 °C.

The results of this analysis showed that there is a variation in comfort indices, even though both references are located in the same borough with the same demographic, geographical, and climatic characteristics.

To better understand this variation, we compared the stations St-Léonard1 and St-Léonard2, which are located respectively in a park and in a parking lot (Figure 6). The temperature curves show that the maximum values were reached during the heatwave (6 September 2023, at 4 p.m.), corresponding to 33.29 °C for St-Léonard1 and 32.59 °C for St-Léonard2, showing a difference of 0.7 °C. According to the temperature difference curve between these two stations, ΔT , the difference can reach 1.67 °C.

To quantify and compare the effect of UHI, the exceedances of comfort thresholds for the different comfort indices used in the analysis were calculated, as shown in Table 5. The thresholds are depicted in Table 6.

This approach was applied throughout the study period from 17 July 2023 to 30 September 2023 (no heatwave period—NHW) and during the heatwave period (HW) from 4 September 2023 to 8 September 2023. We wanted to compare regions with similar characteristics and one major differing factor (Appendix C).

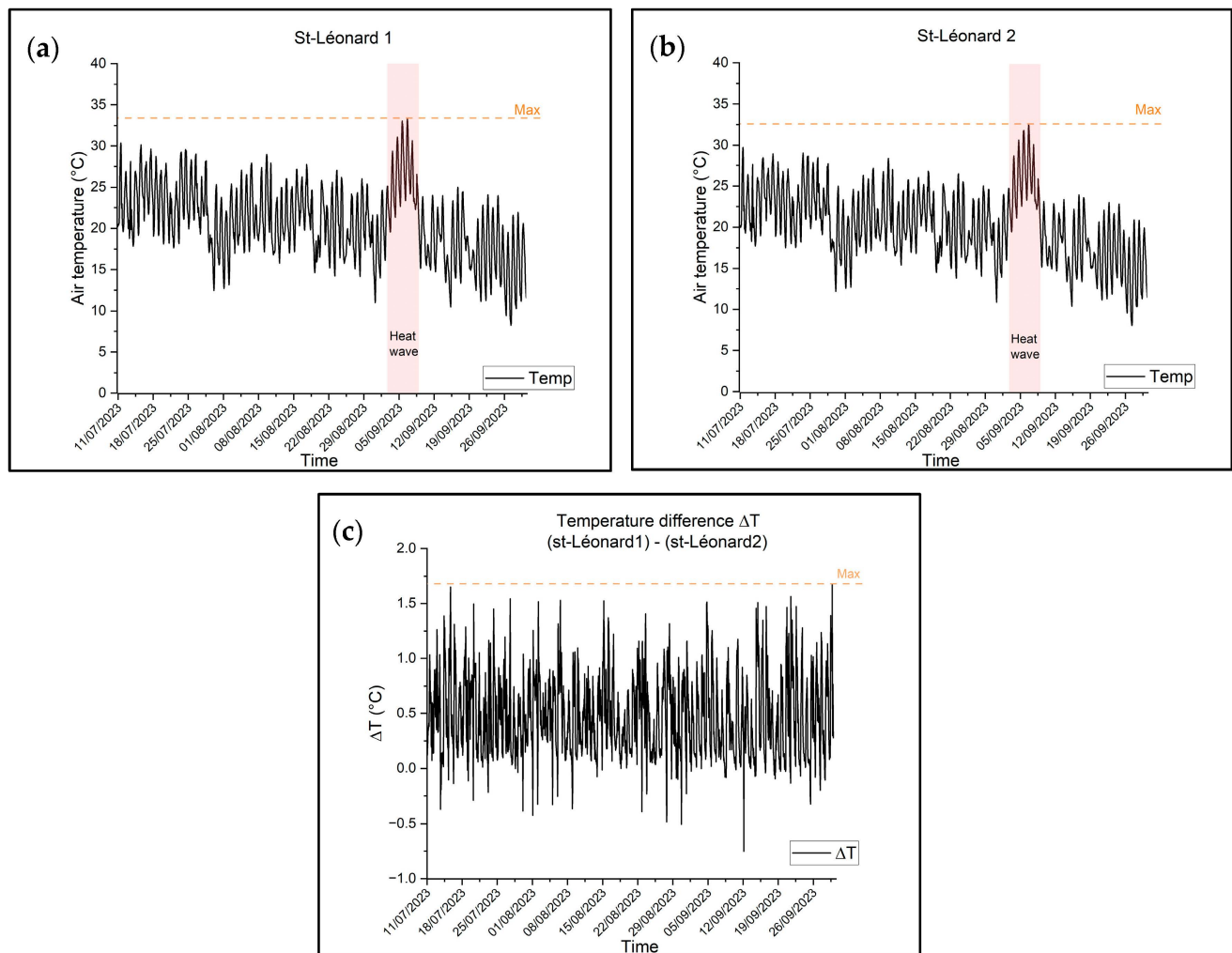


Figure 6. Air temperature profile in Saint-Léonard borough: (a) St-Léonard 1, (b) St-Léonard 2, (c) temperature difference.

Table 5. Thresholds related to comfort indices.

Comfort Index	Threshold	Impact
Humidex	40	The population experiences a lot of discomfort and should avoid heavy exertion.
DI	24	The thermal load is moderately high, people feel very hot, and physical work can be performed with some difficulty.
HI	32	People need to be extremely cautious. There is a possibility of sunstroke, muscle cramps, and heat exhaustion in cases of prolonged exposure and/or physical activity.
THI	26	Almost everyone feels uncomfortable.

In terms of urban density, a comparison was made between 5-Hopital_M-R and 13-Sud-Ouest-1, after which we found that the exceedance percentages for humidex and DI were very similar, while HI and THI for 5-Hopital_M-R were slightly higher than for 13-Sud-Ouest-1. From this, we can assume that density has a minimal impact on UHIs.

Table 6. Exceedance rates during heatwave period.

Station's Name	Period	Exceedance in %			
		Humidex > 40	DI > 24	HI > 32	THI > 26
1-Boise-Peres	NHW	0.00	4.13	0.88	1.75
	HW	0.00	43.33	11.67	23.33
2-Carref_Langelier	NHW	0.33	5.25	1.31	2.90
	HW	5.00	48.33	20.00	34.17
3-CDN-NDG-1	NHW	0.22	2.34	0.44	1.10
	HW	6.67	43.33	13.33	30.83
4-Espace_67	NHW	0.40	6.36	1.25	2.27
	HW	5.83	45.83	18.33	26.67
5-Hopital_M-R	NHW	0.61	6.07	1.54	3.09
	HW	9.17	50.83	23.33	34.17
6-Jean-Drapeau_Etang	NHW	0.00	3.59	0.22	1.06
	HW	0.00	40.83	3.33	15.83
7-Jean-Milot	NHW	0.50	3.53	0.66	1.38
	HW	7.50	33.33	10.00	20.83
8-MHM 1	NHW	0.60	6.09	1.59	3.02
	HW	9.17	53.33	24.17	36.67
9-MHM 2	NHW	0.55	5.76	1.54	3.02
	HW	8.33	50.00	23.33	36.67
10-Outremont 1	NHW	0.55	5.76	1.15	2.19
	HW	8.33	48.33	17.50	30.00
11-Saint-Leonard 1	NHW	0.71	6.41	1.48	3.02
	HW	10.83	50.00	22.50	35.00
12-Saint-Leonard 2	NHW	0.44	4.99	1.15	2.19
	HW	6.67	45.00	17.50	30.00
13-Sud-Ouest-1	NHW	0.61	6.08	1.16	2.82
	HW	9.17	45.83	17.50	31.67
14-VSMPE 1	NHW	0.38	6.36	1.26	3.29
	HW	5.83	50.83	19.17	32.50
15-VSMPE 2	NHW	0.60	5.32	1.21	2.41
	HW	9.17	48.33	18.33	34.17

Concerning the impact of vegetation cover, a comparison was made between 10-Outremont 1 and 11-Saint-Léonard 1, after which we found that the exceedance percentages for all comfort indices for 11-Saint-Léonard 1 were higher than those for 10-Outremont 1. Therefore, we can assume that vegetation cover has a significant impact on UHIs.

When it comes to the impact of proximity to water, a comparison was made between 8-MHM 1 and 2-Carref_Langelier, after which we found that the exceedance percentages for all comfort indices for 8-MHM 1 were higher than those for 2-Carref_Langelier. Hence, we can assume that proximity to water has a significant impact on UHIs. Sainte-Hélène Island presents a unique case with the lowest density, the highest percentage of vegetation cover, and proximity to water bodies.

By comparing the two sensors installed on the island, 6-Jean-Drapeau_Etang and 4-Espace_67, we found a huge difference across all compared indices. This suggests that, despite the regional similarities, the exact location of the sensor can yield very different results. This may be due to the nature of the surfaces adjacent to the sensor and their thermal characteristics.

4. Conclusions and Work Limitations

This study on Montreal's urban heat island (UHI) transcends a mere confirmation of rising urban temperatures, offering critical insights into the nuanced interplay between

urban characteristics and outdoor thermal comfort. Our analysis, uniquely combining surface thermal and air climate data, reveals that Montreal's thermal landscape is significantly shaped by the spatial distribution of its dense urban fabric and the limited extent of its vegetation cover, particularly under specific climatic conditions. Notably, the pronounced exceedance of thermal comfort index thresholds during heatwaves underscores the tangible impact of UHI on the well-being of Montreal's residents, especially in densely populated areas lacking sufficient green infrastructure. This research provides new, localized evidence that quantifies the severity of thermal discomfort during extreme heat events in Montreal, highlighting specific vulnerable regions within the city.

Based on these findings, we recommend a targeted and localized approach to urban planning in Montreal that prioritizes the strategic expansion of green spaces, particularly in densely built-up areas identified as UHI hotspots. This expansion should consider Montreal's existing planning regulations and land use constraints, potentially focusing on underutilized spaces or integrating green infrastructure into new developments. Furthermore, we suggest a feasibility assessment of implementing cool roof and pavement technologies in these vulnerable zones, taking into account the city's fiscal capacities and the specific characteristics of Montreal's building stock and infrastructure. Future research should employ scenario modeling to evaluate the effectiveness and cost-benefit of these localized mitigation strategies under various climate projections for Montreal. Additionally, spatial prioritization frameworks could be utilized to identify the most impactful areas for intervention based on factors like population density, vulnerability, and existing green space deficits. This study lays the groundwork for a more informed and proactive approach to mitigating the adverse effects of UHI in Montreal by highlighting key areas for targeted interventions and emphasizing the need for locally grounded and feasible implementation strategies.

Author Contributions: Y.H.: Investigation; Data curation; Resources; Writing—original draft preparation; Writing—review and editing; Formal analysis; Visualization. A.M.: Methodology; Supervision; Project administration; Validation; Resources; Investigation; Writing—review and editing. W.M.: Methodology; Supervision; Conceptualization; Validation; Writing—review and editing. All authors have read and agreed to the published version of the manuscript.

Funding: This research received no external funding.

Data Availability Statement: No new data were created.

Conflicts of Interest: The authors declare no conflict of interest.

Nomenclature

Abbreviations		SVF	Sky View Factor
UHI	Urban Heat Island	BEM	Building Energy Model
LST	Land surface temperature	WRF	Weather Research and Forecasting
UHI	Urban Heat Island	POS	Percentage of Synchronization
SUHII	Surface UHI intensity	Symbols	
HW	Heat wave	e	Vapor pressure (hPa)
DHW	Dry heat wave	k	The number of factors
MHW	Moist heat wave	RH	Relative humidity (%)
EHY	Extreme heat years	T	Air temperature (°C)
CDH	Cooling degree hours	$T_{dew\ point}$	Dew point temperature (°C)
LCZ	Local climate zone	T_w	Wet-bulb temperature (°C)
EHDE	Extra Hot Day Exposure	t	Time (days)

Appendix A. List of Indices

The literature review allowed us to identify a list of indices used in various studies and research related to our research topic.

Table A1. List of indices.

Index	Formula	Description
Percentage of synchronisation (POS) [15]	$POS = \frac{\sum_{i=1}^{c \cdot m} VO_i}{c \cdot m}$	This index serves the purpose of selecting a representative EHY based on the idea of synchronization of the outdoor and indoor extreme years: c = number of extreme years m = number of building configurations i = building configuration VO = (1 or 0) extreme outdoor year in the indoor extreme year.
Temperature based index (severity) [15]	$WCDH = \sum_{i=1}^N \sum_{t=1}^{24} (T_0 - T_{cu})^2$	This index calculates the severity of the heat event by weighting the number of cooling degree hours. T_0 = the hourly daily operative temperature T_{cu} = the adaptive threshold temperature
Thermal based index (severity) [15]	$SETH = \sum_N SETH_d + SETH_n$ $= \sum_{dayhour} [t - SET - t - SET_d]^+ + \sum_{nighthour} [t - SET - t - SET_n]^+$	This index calculates the severity of the heat event. N = duration in days of heat event $SETH_d$ = severity during daytime $SETH_n$ = severity during nighttime $t - SET$ = standart effective temperature (confort index) $t - SET_d = 30^\circ\text{C}$, $SET_n = 26^\circ\text{C}$ outdoor and 30°C indoor If $SETH_d$ surpass 4C for two successive days, it's a heat event.
Rural-ring [14]	$UHI_{RR} = T_{Urban} - T_{Rural}$	The UHI is calculated as the temperature difference between urban areas and surrounding rural areas
Urban-increment [14]	$UHI_{UI} = T_{Urban} - T_{Cropland}$	The UHI is calculated as the temperature between the urban land-cover of the cities and another in which the urban land-cover is replaced by croplands
Actual moisture availability [14]	$\theta_{actual} = \theta \cdot F_{Vegetation}$	(θ) = The volumetric soil moisture in the top surface layer $F_{Vegetation}$ = the average green area fraction
Surface energy balance [14]	$Q^* = Q_H + Q_E + \Delta Q_S$	The net amount of income and outcome energy of a wave can be split into three parts, including the sensible heat flux (QH), latent heat flux (QE), and net heat storage flux (ΔQ_S)
Cooling degree-hours [16]	$CDH = \sum_{i=1}^N (T_i - T_b) \cdot \delta$	CDH refers to the extent of cooling demand in degree hours for a chosen base temperature and is defined as the cumulative sum of the temperature difference between the hourly outside reference and base temperature T_i = hourly temperature ($^\circ\text{C}$), T_b = base temperature ($^\circ\text{C}$), $\delta = 1$, when $T_i > T_b$ and $\delta = 0$, when $T_i < T_b$
Surface UHI intensity [11]	$SUHII = LST_{Urban} - LST_{rural}$	
Relationship between the SUHI and the independent parameters [11]	$SUHII_{model} = a0 + (a1 \times NDBI) + (a2 \times NDVI) + (a3 \times NDWI) + (a4 \times Distance) + (a5 \times Density)$	NDBI is the mean brightness, NDVI is the mean greenness, NDWI is the mean wetness in urban areas. Distance is the Euclidean distance of the city center from the coastline. Density is the population density of each city.
Humidex [33]	$Humidex = T + h$ $h = (0.5555) \times (e - 10.0);$ $e = \text{Vaport pressure (hPa):}$ $e = 6.11 \times \exp[5417.7530 \times ((1 \div 273.15) - (1 \div \text{Dew} - \text{point}))]$ $\text{Dew point is expressed in kelvins (temperature en K = temperature in } ^\circ\text{C} + 273.15)$	From 20 to 29: A little discomfort. From 30 to 39: Some discomfort. From 40 to 45: A lot of discomfort; avoid effort. Above 45: Danger; possible heat stroke [34].

Table A1. Cont.

Index	Formula	Description
Wet-bulb temperature (T_w) [13]	$T_w = T \times \left(\frac{\tan(0.1520 \times (RH + 8.3137)^{1/2}) + \tan(T + RH) - \tan(RH - 1.676) + 0.0039 \times RH^{2/3} \times \tan(0.0231 \times RH) - 4.6860}{1} \right)$	
Discomfort index [13]	$DI = 0.5(T_w + T)$	<p>Under 22: No heat stress is encountered.</p> <p>22–24: Most people feel a mild sensation of heat.</p> <p>24–28: The heat load is moderately heavy, people feel very hot, and physical work may be performed with some difficulties.</p> <p>Above 28: The heat load is considered severe, and people engaged in physical work are at increased risk for heat illness [26].</p>
Heat index [4] A corrigier	$HI = -8.7847 + 1.6114 \times T + 2.3385 \times RH - 0.1461 \times T \times RH - 1.2308 \times 10^{-2} \times T^2 - 1.6425 \times 10^{-2} \times RH^2 + 2.2117 \times 10^{-3} \times T^2 \times RH + 7.2546 \times 10^{-4} \times T \times RH^2 - 3.5820 \times 10^{-6} \times T^2 \times RH^2, \&(T > 20)$	<p>Relative humidity (RH, %):</p> <p>27–32: Caution; Fatigue possible with prolonged exposure and/or physical activity.</p> <p>32–41: Extreme caution; Sunstroke, muscle cramps, and/or heat exhaustion possible with prolonged exposure and/or physical activity.</p> <p>41–54: Danger; Sunstroke, muscle cramps, and/or heat exhaustion likely. Heatstroke possible with prolonged exposure and/or physical activity.</p> <p>≥54: Extreme danger; Heat stroke or sunstroke likely [25].</p>
Hot day exposure [8]	$HDE_i = HDF_i \times POP_i$	<p>HDE_i is the hot-day exposure of point i,</p> <p>HDF_i is the annual number of hot days at point i,</p> <p>POP_i is the population of point i.</p>
Poverty related heat exposure [8]	$HDE_p = \begin{cases} HDF \times POP, GDP - PT < 0 \\ 0, GDP - PT \geq 0 \end{cases}$	
Extra heat day exposure [17]	$EHDE_i = \begin{cases} (HDF_i - HDF_{LCZD})POP_i, HDF_i - HDF_{LCZD} > 0 \\ 0, HDF_i - HDF_{LCZD} \leq 0 \end{cases}$	
The sum of EHDE [17]	$EHDE = \sum_{j \in LCZ1, 2, 3, \dots, 10} EHDE_{LCZj}$	Total EHDE due to the UHI effect is estimated as the sum of the EHDE for all built-type LCZs
EHDE intensity [17]	$I_{LCZj} = EHDE_{LCZj} / Area_j$	The EHDE intensity of LCZ, I_{LCZj} , is defined as the ratio of EHDE to area in the LCZj
Integral Index of Connectivity (IIC) [26]	$IIC = \frac{\sum_{i=1}^n \sum_{j=1}^n \left(\frac{a_i a_j}{1 + m_{ij}} \right)}{A_L^2}$	<p>The Integral Index of IIC and PC serve to gauge the thermal landscape connectivity of UHI sources. dI index serves to identify crucial heat sources.</p> <p>n = the total number of heat source patches;</p> <p>$a_i a_j$ = represent the area of patches;</p> <p>m_{ij} = the number of connections between patches i and j</p> <p>A_L is the total area of the landscape research area;</p> <p>I = the connectivity index value when the landscape contains landscape elements;</p> <p>I_{remove} = is the index value after removing the landscape element.</p>
Probability of Connectivity (PC) [26]	$PC = \frac{\sum_{i=1}^n \sum_{j=1}^n a_i a_j P_{ij}^s}{A_L^2}$	
Patch importance (dI) [26]	$dI(\%) = \frac{I - I_{remove}}{I} \times 100\%$	
Plan area density [25]	$\gamma_p = \frac{b}{b + w}$	<p>This index helps calculate the SVF on 2d plans</p> <p>H_m = building height,</p> <p>γ_p = plan area density,</p> <p>γ_f = frontal area density,</p> <p>b = building size,</p> <p>w = street width.</p>

Table A1. Cont.

Index	Formula	Description
Frontal area density [25]	$\gamma_f = \frac{Hm}{b+w}$	
Calculating Sky view factor [25]	$F1 = 1 - Frw1 - Frw2$ $Frw = \frac{1}{2} \left(1 + x - \sqrt{1 + x^2} \right)$ $x = \frac{h}{w}$	F1 = is the sum of street-to-wall view factors (Frw) subtracted from unity, h = the wall height and w is the street width.
Temperature-humidity index (THI) [30]	$THI = 0.8T + 0.2t \times \left(\frac{RH}{100} \right)$	This index helps determine the effect of relative humidity and air temperature on thermal comfort. THI of about 21 °C is associated with most people feeling comfortable; at a THI of about 24 °C around half of the population experiences some form of thermal stress; when THI reaches 26 °C, almost all feel uncomfortable [37].

Appendix B. Demographic Distribution

The table below shows the demographic distribution of the Montreal agglomeration according to the most recent census (2021).

Table A2. Population Growth in the Montreal Agglomeration 2016–2021.

Borough	Population in 2021	Variation (%) 2016–2021	Area (km ²)	Density (hab./km ²)
MONTREAL AGGLOMERATION	2,004,265	3.20	498.29	4022
City of Montreal	1,762,949	3.42	364.74	4834
Ahuntsic–Cartierville	135,336	0.81	24.16	5602
Anjou	43,243	1.04	13.68	3161
Côte-des-Neiges–Dame-de-Grâce	170,583	2.44	21.44	7956
Lachine	46,428	4.36	17.72	2620
LaSalle	82,235	7.00	16.27	5054
Plateau–Mont-Royal	105,813	1.74	8.13	13,015
Sud-Ouest	84,553	8.19	15.68	5392
L’Île-Bizard–Sainte-Geneviève	18,885	2.56	23.60	800
Mercier–Hochelaga–Maisonneuve	140,627	3.38	25.41	5534
Montreal-Nord	88,471	5.03	11.05	8006
Outremont	24,629	2.82	3.85	6397
Pierrefonds–Roxboro	70,382	1.57	27.06	2601
Rivière-des-Prairies–Pointe-aux-Trembles	107,941	1.12	42.28	2553
Rosemont–La-Petite-Patrie	141,813	1.59	15.85	8947
Saint-Laurent	102,104	3.31	42.77	2387
Saint-Léonard	79,495	1.52	13.49	5893
Verdun	70,377	1.66	9.72	7244
Ville-Marie	104,944	17.69	16.52	6353
Villeray–Saint-Michel–Parc-Extension	145,090	0.86	16.49	8799
City of Baie-D’Urfé	3764	−1.54	6.01	626
City of Beaconsfield	19,277	−0.24	10.98	1756
City of Côte-Saint-Luc	34,504	6.34	6.94	4972
City of Dollard-des-Ormeaux	48,403	−1.01	15.17	3191
City of Dorval	19,302	1.70	20.85	926
City of Hampstead	7037	0.92	1.79	3940
City of Kirkland	19,413	−3.66	9.62	2017
City of Montreal-Est	4394	14.13	12.46	353
City of Montreal-Ouest	5115	1.29	1.40	3643
City of Mont-Royal	20,953	3.34	7.65	2741
City of Pointe-Claire	33,488	6.72	18.84	1777
City of Sainte-Anne-de-Bellevue	5027	1.39	10.55	476
City of Senneville	951	3.26	7.47	127
City of Westmount	19,658	−3.22	4.02	4892

Appendix C. Demographic Distribution

Table A3. Demographic Distribution.

Borough	Population in 2021	Density (hab/km ²)	Vegetation Cover (%)	Sensors	Proximity to the Coast (km)
Côte-des-Neiges–Notre-Dame-de-Grâce	170,583	7956	9.88	3-CDN-NDG-1	6.6
Rosemont–La-Petite-Patrie	141,813	8947	15.24	1-Boise-Peres	3.2
Ville-Marie:				5-Hopital_M-R	3.3
Sainte-Hélène Island	N/A	N/A	70.54	4-Espace_67	0.16
				6-Jean-Drapeau_Etang	0.14
Mercier–Hochelaga–Maisonnette	140,627	5534	8.27	7-Jean-Milot	4.6
				8-MHM 1	1.0
Outremont	24,629	6397	24.5	9-MHM 2	1.3
Le Sud-Ouest	84,553	5392	11.37	10-Outremont 1	5.5
Villeray–Saint-Michel–Parc-Extension	145,090	8799	14.66	13-Sud-Ouest-1	2.1
				14-VSMPE 1	3.4
				15-VSMPE 2	2.5
Saint-Léonard	79,495	5893	5.05	11-St-Léonard 1	3.8
				12-St-Léonard 2	3.8
				2-Carref_Langelier	5.0

References

- Manoli, G.; Fatichi, S.; Schlapfer, M.; Yu, K.L.; Crowther, T.W.; Meili, N.; Burlando, P.; Katul, G.G.; Zeid, E.B. Magnitude of urban heat islands largely explained by climate and population. *Nature* **2019**, *573*, 55–60. [\[CrossRef\]](#) [\[PubMed\]](#)
- Santamouris, M. On the energy impact of urban heat island and global warming on buildings. *Energy Build.* **2014**, *82*, 100–113. [\[CrossRef\]](#)
- He, B.J.; Zhao, D.X.; Dong, X.; Xiong, K.; Feng, C.; Qi, Q.L.; Darko, A.; Sharifi, A.; Pathak, M. Perception, physiological and psychological impacts, adaptive awareness and knowledge, and climate justice under urban heat: A study in extremely hot-humid Chongqing. *China. Sustain. Cities Soc.* **2022**, *79*, 103685. [\[CrossRef\]](#)
- Fadhil, M.; Hamoodi, M.N.; Ziboon, A.R.T. Mitigating urban heat island effects in urban environments: Strategies and tools. *IOP Conf. Ser. Earth Environ. Sci.* **2023**, *1129*, 012025. [\[CrossRef\]](#)
- Guo, C.; Lanza, K.; Li, D.; Zhou, Y.; Aunan, K.; Loo, B.P.Y.; Lee, J.K.W.; Luo, B.; Duan, X.; Zhang, W.; et al. Impact of heat on all-cause and cause-specific mortality: A multi-city study in Texas. *Environ. Res.* **2023**, *224*, 115453. [\[CrossRef\]](#)
- Ignjačević, P.; Botzen, W.; Estrada, F.; Daanen, H.; Lupi, V. Climate-induced mortality projections in Europe: Estimation and valuation of heat-related deaths. *Int. J. Disaster Risk Reduct.* **2024**, *111*, 104692. [\[CrossRef\]](#)
- Mitchell, D. Climate attribution of heat mortality. *Nat. Clim. Chang.* **2021**, *11*, 467–468. [\[CrossRef\]](#)
- Debbage, N.; Shepherd, J.M. The urban heat island effect and city contiguity. *Comput. Environ. Urban Syst.* **2015**, *54*, 181–194. [\[CrossRef\]](#)
- Qian, Y.; Chakraborty, T.C.; Li, J.F.; Li, D.; He, C.L.; Sarangi, C.; Chen, F.; Yang, X.C.; Leung, L.R. Urbanization impact on regional climate and extreme weather: Current understanding, uncertainties, and future research directions. *Adv. Atmos. Sci.* **2022**, *39*, 819–860. [\[CrossRef\]](#)
- Oke, T.R. The energetic basis of the UHI. *Q. J. R. Meteorol. Soc.* **1982**, *108*, 1–24.
- Firozjaei, M.K.; Sedighi, A.; Mijani, N.; Kazemi, Y.; Amiraslani, F. Seasonal and daily effects of the sea on the surface UHI intensity: A case study of cities in the Caspian Sea Plain. *Urban Clim.* **2023**, *51*, 101603. [\[CrossRef\]](#)
- Zhao, L.; Oppenheimer, M.; Zhu, Q.; Baldwin, J.W.; Ebi, K.L.; Bou-Zeid, E.; Guan, K.; Liu, X. Interactions between UHIs and heat waves. *Environ. Res. Lett.* **2018**, *13*, 034003. [\[CrossRef\]](#)
- Kim, D.-H.; Park, K.; Baik, J.-J.; Jin, H.-G.; Han, B.-S. Contrasting interactions of UHIs with dry and moist heat waves and their implications for urban heat stress. *Urban Clim.* **2024**, *56*, 102050. [\[CrossRef\]](#)
- Shu, C.; Gaur, A.; Wang, L.; Lacasse, M. Evolution of the local climate in Montreal and Ottawa before, during and after a heatwave and the effects on UHIs. *Sci. Total Environ.* **2023**, *890*, 164497. [\[CrossRef\]](#)
- Ji, L.; Laouadi, A.; Shu, C.; Gaur, A.; Lacasse, M.; Wang, L. Evaluating approaches of selecting extreme hot years for assessing building overheating conditions during heatwaves. *Energy Build.* **2022**, *245*, 111610. [\[CrossRef\]](#)
- Errebai, F.B.; Strebel, D.; Carmeliet, J.; Derome, D. Impact of UHI on cooling energy demand for residential building in Montreal using meteorological simulations and weather station observations. *Energy Build.* **2022**, *273*, 112410. [\[CrossRef\]](#)
- Yu, W.; Yang, J.; Sun, D.; Ren, J.; Xue, B.; Sun, W.; Xiao, X.; Xia, J.C.; Li, X. How UHI magnifies hot day exposure: Global unevenness derived from differences in built landscape. *Sci. Total Environ.* **2024**, *945*, 174043. [\[CrossRef\]](#)

18. Alizadeh, M.R.; Abatzoglou, J.T.; Adamowski, J.F.; Prestemon, J.P.; Chittoori, B.; Akbari Asanjan, A.; Sadegh, M. Increasing heat-stress inequality in a warming climate. *Earth's Future* **2022**, *10*, e2021EF002488. [CrossRef]
19. Tuholske, C.; Caylor, K.; Funk, C.; Verdin, A.; Sweeney, S.; Grace, K.; Peterson, P.; Evans, T. Global urban population exposure to extreme heat. *Proc. Natl. Acad. Sci. USA* **2021**, *118*, e2024792118. [CrossRef]
20. Wang, Y.; Zhao, N.; Yin, X.; Wu, C.; Chen, M.; Jiao, Y.; Yue, T. Global future population exposure to heatwaves. *Environ. Int.* **2023**, *178*, 108049. [CrossRef]
21. Stewart, I.; Oke, T. Local climate zones for urban temperature studies. *Bull. Am. Meteorol. Soc.* **2012**, *93*, 1879–1900. [CrossRef]
22. Welegedara, N.P.Y.; Agrawal, S.K.; Lotfi, G. Exploring spatiotemporal changes of the UHI effect in high-latitude cities at a neighbourhood level: A case of Edmonton, Canada. *Sustain. Cities Soc.* **2023**, *90*, 104403. [CrossRef]
23. Hurdud, A.; Ermida, S.L.; Trigo, I.F.; DaCamara, C.C. Importance of temporal dimension and rural land cover when computing surface UHI intensity. *Urban Clim.* **2024**, *56*, 102013. [CrossRef]
24. Deng, X.; Yu, W.; Shi, J.; Huang, Y.; Li, D.; He, X.; Zhou, W.; Xie, Z. Characteristics of surface UHIs in global cities of different scales: Trends and drivers. *Sustain. Cities Soc.* **2024**, *107*, 105483. [CrossRef]
25. Touchaei, A.G.; Wang, Y. Characterizing UHI in Montreal (Canada)—Effect of urban morphology. *Sustain. Cities Soc.* **2015**, *19*, 395–402. [CrossRef]
26. Zhao, Z.; Li, W.; Zhang, J.; Zheng, Y. Constructing an UHI network based on connectivity perspective: A case study of Harbin, China. *Ecol. Indic.* **2024**, *159*, 111665. [CrossRef]
27. Shamsaei, M.; Carter, A.; Vaillancourt, M. Using urban and demolition waste materials to alleviate the negative effect of pavements on the UHI: A laboratory, field, and numerical study. *Case Stud. Urban Mater.* **2024**, *20*, e03346.
28. Ghaseminasab, M.; Berraha, Y.; Carter, A.; Vaillancourt, M. Caractérisation des paramètres thermiques de mélanges d'enrobé bitumineux contenant différents matériaux de post-consommation, à l'aide de deux méthodes d'essai thermique. *Via Bitume* **2023**, *18*, 46–51.
29. Faragallah, R.N.; Ragheb, R.A. Evaluation of thermal comfort and UHI through cool paving materials using ENVI-Met. *Ain Shams Eng. J.* **2022**, *13*, 101609. [CrossRef]
30. Cortes, A.; Rejuso, A.J.; Santos, J.A.; Blanco, A. Evaluating mitigation strategies for UHI in Mandaue City using ENVI-met. *J. Urban Manag.* **2022**, *11*, 97–106. [CrossRef]
31. Morales-Gonzalez, I.; Verichev, K.; Carpio, M. Efficiency assessment for the UHI mitigation measures in a city with an oceanic climate during the summer period: Case of Valdivia, Chile. *Urban Clim.* **2024**, *55*, 101897. [CrossRef]
32. Zhao, Q.; Tao, L.; Song, H.; Lin, Y.; Ji, Y.; Geng, J.; Liu, J. Mitigation pathways of urban heat islands and simulation of their effectiveness from a perspective of connectivity. *Sustain. Cities Soc.* **2025**, *124*, 106300. [CrossRef]
33. Masterton, J.M.; Richardson, F.A. *Humidex A. Method of Quantifying Human Discomfort Due to Excessive Heat and Humidity*; Environment Canada: Downsview, ON, Canada, 1979.
34. Canadian Centre for Occupational Health and Safety. Available online: https://www.ccohs.ca/oshanswers/phys_agents/humidex.html (accessed on 10 November 2024).
35. Blazejczyk, K.; Epstein, Y.; Jendritzky, G.; Staiger, H.; Tinz, B. Comparison of UTCI to selected thermal indices. *Int. J. Biometeorol.* **2012**, *56*, 515–535. [CrossRef] [PubMed]
36. Epstein, Y.; Moran, D.S. Thermal Comfort and the Heat Stress. *Ind. Health* **2006**, *44*, 388–398. [CrossRef]
37. Lia, X.-X.; Norford, L.K. Evaluation of cool roof and vegetations in mitigating UHI in a tropical city, Singapore. *Urban Clim.* **2015**, *16*, 59–74. [CrossRef]
38. Available online: <https://www.thecanadianencyclopedia.ca/fr/article/montreal-1> (accessed on 15 November 2024).
39. Available online: <https://donnees.montreal.ca/dataset> (accessed on 10 November 2024).
40. Available online: <https://www.onsetcomp.com/> (accessed on 16 November 2024).
41. Available online: <http://ville.montreal.qc.ca/portal/> (accessed on 16 November 2024).
42. Available online: <https://www.canada.ca/fr/environnement-changement-climatique/services/changements-climatiques/centre-canadien-services-climatiques/afficher-telecharger/documentation-technique-normales-climatiques.html> (accessed on 7 October 2024).
43. Available online: <https://bter.maps.arcgis.com/apps/webappviewer/index.html?id=157cde446d8942d7b4367e2159942e05> (accessed on 7 January 2024).

Disclaimer/Publisher's Note: The statements, opinions and data contained in all publications are solely those of the individual author(s) and contributor(s) and not of MDPI and/or the editor(s). MDPI and/or the editor(s) disclaim responsibility for any injury to people or property resulting from any ideas, methods, instructions or products referred to in the content.